Musculotopic organization of the motor neurons supplying the mouse hindlimb muscles — a quantitative study using Fluoro-Gold retrograde tracing

Tímea Bácskai[1*], Zoltán Rusznák[1*], George Paxinos[1,2], and Charles Watson[1,3]

[1]Neuroscience Research Australia, Sydney, NSW, 2031, Australia
[2]The University of New South Wales, Sydney, NSW, 2052, Australia
[3]Faculty of Health Sciences, Curtin University, Perth, WA, 6845, Australia

[*]T. Bácskai and Z. Rusznák have made an equal contribution to this paper.

Corresponding author:
Dr Charles Watson
Curtin University
Shenton Park Health Research Campus
GPO Box U1987
Perth, WA, 6845 Australia
Tel: +61 8 9266 1640
Fax: +61 8 9266 1650
Email: c.watson@curtin.edu.au

Abstract

We have mapped the motor neurons (MNs) supplying the major hindlimb muscles of transgenic (C57/BL6J-ChAT-EGFP) and wild-type (C57/BL6J) mice. The fluorescent retrograde tracer Fluoro-Gold was injected into 19 hindlimb muscles. Consecutive transverse spinal cord sections were harvested, the MNs counted, and the MN columns reconstructed in 3D. Three longitudinal MN columns were identified. The dorsolateral column extends from L4 to L6 and consists of MNs innervating the crural muscles and the foot. The ventrolateral column extends from L1 to L6 and accommodates MNs supplying the iliopsoas, gluteal, and quadriceps femoris muscles. The middle part of the ventral horn hosts the central MN column, which extends between L2–L6 and consists of MNs for the thigh adductor, hamstring, and quadratus femoris muscles. Within these longitudinal columns, the arrangement of the different MN groups reflects their somatotopic organization. MNs innervating muscles developing from the dorsal (e.g., quadriceps) and ventral muscle mass (e.g., hamstring) are situated in the lateral and medial part of the ventral gray, respectively. MN pools belonging to proximal muscles (e.g., quadratus femoris and iliopsoas) are situated ventral to those supplying more distal ones (e.g., plantar muscles). Finally, MNs innervating flexors (e.g., posterior crural muscles) are more medial than those belonging to extensors of the same joint (e.g., anterior crural muscles). These data extend and modify the MN maps in the recently published atlas of the mouse spinal cord and may help when assessing neuronal loss associated with MN diseases.

Keywords: Hindlimb, spinal cord, motor neuron, retrograde tracing, musculotopic organization, 3D modeling

Introduction

Motor neurons (MNs) form the final link between the motor cortex and skeletal muscles. We have mapped the topography and determined the number of MNs innervating limb muscles because we believe that these baseline data are important in a number of ways. Firstly, knowing the localization of the MN groups is vital for an understanding of the organization of this part of the motor system. Secondly, knowledge of the exact location of the MN groups is useful for designing and conducting electrophysiology experiments aimed at studying the motor supply of various muscles of the limbs. Thirdly, detailed information about the size and localization of the MN groups is important to the understanding of the pathogenesis, time course, symptoms, and nature of specific diseases targeting MNs, such as amyotrophic lateral sclerosis (ALS). Since *in vivo* labeling, mapping, and investigation in the human spinal cord is not technically possible, one must extrapolate from information available from the experimental animal studies.

There are several established mouse models of ALS, which allow assessment of the MN loss accompanying the development of the disease. Hitherto, ALS research on animal models has focused on the superoxide dismutase 1 (SOD1) G93A 'gain-of-function' transgenic mouse strain (Gurney et al. 1994). $SOD1^{G93A}$ mice demonstrate MN loss resembling that seen in human ALS patients, but it is still not clear how the altered function of SOD1 results in MN loss (see e.g., Beckman et al. 1993; Wiedau-Pazos et al. 1996). Nevertheless, $SOD1^{G93A}$ transgenic mice have been extensively used in ALS research worldwide. In addition, new animal models have also become available, such as mouse strains having mutations at other points of SOD1, in 'transactivating response element DNA binding protein-43' (TDP-43), in Fused in Sarcoma/Translocated in Liposarcoma (FUS/TLS), or mice having diminished activity of the enzyme D-amino-acid oxidase (e.g., Kwiatkowski et al. 2009; Mackenzie et al. 2010; Joyce et al. 2011; Sasabe et al. 2012). Regardless of the nature of the mouse model, however, precise knowledge of the expected number of MNs belonging to the individual MN pools would be important for quantitative analysis of the MN loss associated with ALS and objective determination of the effectiveness of potential therapies. So far, in mouse models of ALS, damage to MNs has been assessed with a number of indirect measurements, including rotarod testing, footprint analysis, grip strength analysis, wire hang test, paw grip endurance, monitoring of body weight, and determination of the mass of selected muscles. Although these tests can provide valuable background information about some aspects of ALS, they are difficult to standardise. Some

studies have attempted to count MNs using histological sections of the spinal cord but these techniques suffer from a number of technical limitations. A problem facing all MN counting approaches is that not all MNs are affected at the same time — in $SOD1^{G93A}$ mice, for example, lumbar MNs have been shown to deteriorate earlier than cervical ones (Azzouz et al. 2004).

In our previous article we have reported on the distribution and size of MN pools innervating muscles of the forelimbs and shoulder girdle in C57BL/6J mice (Bácskai et al. 2012). In the present work we extend our observations to MN pools of the lumbar spinal cord. The interpretation of spinal MN topography is complicated by a number of factors. Firstly, while some MN groups form distinct cluster, many have no clear borders and may overlap with MNs supplying a different muscle. Secondly, accidental spread of tracer to adjacent muscles may blur the pattern of MN topography. Thirdly, interstrain differences, including differences in the segmental distribution of some of the MN pools, may be a significant source of variation. For these reasons, we chose the retrograde tracer Fluoro-Gold (FG) and we reconstructed our results in 3D from a study of serial sections. We chose the C57BL mouse strain because of its importance in gene targeting experiments. We injected FG into 19 muscles of the hindlimb, mapped the location of the various MN groups, and we have counted the number of MNs innervating the individual muscles. The results of this study extend and modify the data presented in a recently published atlas of the mouse spinal cord (Watson et al. 2009a*).*

Materials and Methods

1. Animals

Most experiments were carried out on B6.Cg-Tg(RP23-268L19-EGFP)2Mik/J transgenic mice, male and female, 8 weeks (21–25 g), n = 27, referred hereafter as ChAT-EGFP (choline acetyltransferase-enhanced green fluorescent protein), obtained from The Jackson Laboratory (Bar Harbour, ME, USA). In some cases, experiments were carried out on wild-type C57/BL6 mice as well, 8–10 weeks (21–25 g, n = 10), obtained from the Animal Resources Centre (Canning Vale, WA, Australia). All experimental procedures were in accord with the Australian Code for the Care and Use of Animals in Research, and approved by the Animal Care and Ethics Committee of The University of New South Wales (ACEC No. 11/75A).

2. Surgery and retrograde tracing

The major steps of the MN labeling were the same as described in our recent article (Bácskai et al. 2012). In short, both ChAT-EGFP and wild-type mice were anesthetized with an intraperitoneal injection of ketamine (80 mg/kg) and xylazine (5 mg/kg). MNs were labeled with FG (Fluorochrome, Denver, CO, USA) diluted to 5% with distilled water. The FG solution was kept in dark, airtight containers in a refrigerator (4 °C) until used. All FG solution aliquots were used before their expiry date (6 months). Separate injections were made into the (1) *gluteal muscle group* (consisting of the gluteus superficialis and medius), (2) *hamstring group* (biceps femoris, semitendinosus, and semimembranosus), (3) *adductor group* (adductor magnus and longus, gracilis, and pectineus), (4) *quadriceps group* (quadriceps femoris), (5) *ischiotrochanteric group* (quadratus femoris), (6) *iliacus group* (iliopsoas), (7) *posterior crural group* (both superficial and deep muscles), (8) *anterior crural group* (both superficial and deep muscles), (9) *lateral crural group* (peroneus longus and brevis) and (10) *foot*. The muscles were exposed by incision and retraction of the skin under surgical microscope (Zeiss Stereomicroscope Stemi DV4; Zeiss, Oberkochen, Germany). To avoid inadvertent leakage of the tracer, the fascia of each injected muscle was left intact. In most mice, different muscles were labeled on the left and right side, since preliminary experiments confirmed that all connections were ipsilateral. Each muscle was injected in at least three mice. Identification of the targeted muscles was based on descriptions presented in Green (1959) and Hebel and Stromberg (1976), supplemented by our identification of

important anatomical landmarks (e.g., femoral artery, sciatic or femoral nerve), and the precise origin and insertion of each of the identified muscles.

The FG solution was injected using a 5 µl Hamilton syringe (inner diameter = 0.33 mm; Hamilton Company, Reno, NV, USA). The tracer was injected slowly at multiple sites in each muscle, until the labeled muscle became distinctly colored, ensuring that the tracer filled its entire mass. Depending on the size of the muscle, the amount of FG applied was between 1.5 and 5 µl over a period of 2–5 minutes. In the cases of muscles with multiple heads, each head was injected separately or simultaneously. If leakage was noted during the tracer injection, the excess solution was immediately wiped away. After removing the needle from the muscle, the injection site was washed out with saline then covered by wax to minimize spread of FG to adjacent muscles. Examples of cases in which we judged the labeling to be complete, incomplete, or subject to excessive leakage of the FG into a neighboring muscle are shown in Fig 1. Following injections, the skin was sutured and tetracycline was sprayed over the incision.

3. Tissue processing and localization of the motor neurons

After a survival time of 6 days (Haenggeli and Kato 2002), mice were anesthetized with a lethal dose of pentobarbitone sodium (0.24 mg/g body weight) and transcardially perfused with 0.9% saline, followed by 4% paraformaldehyde prepared in 0.1 M phosphate buffer (*pH* 7.4, 4 °C).

After opening the vertebral canal and dura mater, spinal segments were carefully identified by dissecting the dorsal roots of the spinal nerves to their point of origin into the spinal cord. Because mice, even inbred mice, may have five, rather than six, lumbar vertebrae in some cases (McLaren and Michie 1954 and 1958), we examined the lumbar vertebral column after removal of the spinal cord to ensure that there were six lumbar vertebrae between the last rib and the sacrum. After removal of the spinal cord, a portion of each spinal cord containing segments T13–S1 was post-fixed overnight. For cryoprotection, the cords were placed in 30% sucrose buffer (4 °C, overnight). Serial transverse sections were cut using a Leica CM 1950 cryostat (Leica Microsystems GmbH, Wetzlar, Germany) at a thickness of 40 µm. Consecutive sections were collected, mounted, and coverslipped with Dako Fluorescence Mounting Medium (Dako, Campbellfield, Australia).

Further identification of the individual spinal cord segments was based on the morphology of the spinal gray matter according to the mouse spinal cord atlas of Watson et al. (2009a).

4. Cell counting and spinal cord reconstruction

The sections were examined using a fluorescence microscope (BX51, Olympus, Tokyo, Japan) and photographed using an attached camera (AxioCam HRc, Zeiss). All sections containing labeled cells were mapped and the lumbar spinal cords were reconstructed in 3D using Neurolucida software (v10 with Zeiss Imager M2 microscope, MBF Bioscience Inc., Vermont, USA). All labeled MNs (including both α and γ motor neurons) having well-defined nuclear area were counted on every second serial section using the ×20 objective of the fluorescence microscope. The total number of MNs innervating any particular muscle was determined by counting the number of labeled MN profiles along the entire length of the relevant spinal cord segments. To compensate for possible double counting of profiles, the actual cell numbers were corrected using the Abercrombie formula (Abercrombie 1946, Bácskai et al. 2012).

Results

1. General observations

In native (i.e., non-labeled) spinal cord sections prepared from ChAT-EGFP mice, MNs could be identified on the basis of their ChAT positivity, which was evidenced by their strong green fluorescence (Fig. 2). As expected from our previous study of cervical spinal cord (Bácskai et al. 2012), the MNs formed relatively distinct cell clusters spread over 5 to 6 spinal cord segments (in this case mostly from L1 to L6). By considering the rostrocaudal, dorsoventral, and mediolateral positions of the individual MN groups, we were able to identify specific hindlimb muscle groups.

To ensure accurate classification of the MNs and to determine the number of cells innervating the individual muscles of the hindlimb, FG injections were always applied into individual muscles. FG-labeled cells could be easily identified on the basis of the strong fluorescence signal they emitted when visualized under the microscope. Generally, labeled MNs had their cell bodies and proximal processes filled with FG granules, whereas their nuclei remained unlabeled (Fig. 3). The majority of the MNs had large, polygonal cell bodies with a number of dendrites (Fig. 3a–b). About 10% of the labeled MNs had smaller and more spherical cell bodies, which generally had only two visible dendrites (Fig. 3c–e). The large and small MNs were classified as α-motor neurons and γ-motor neurons, respectively.

2. Organization of the motor neurons supplying the hindlimb

We injected 10 different groups of muscles with FG. In some cases all muscles associated with a muscle group were labeled (e.g., quadriceps femoris), while in other cases only the most easily accessible and/or biggest muscles were injected (e.g., ischiotrochanteric or iliacus group). Each muscle was labeled in at least three mice. While the number of MNs innervating the individual muscles was somewhat variable, their rostrocaudal extent was similar. The latter observation suggested that leakage of FG and inadvertent labeling of other MNs was minimal.

In the subsequent sections, we give a detailed account of the distribution of the individual MN groups. An overview of all relevant data is provided in Table 1 and Table 2. The associated figures (Figs. 4–6) demonstrate the number and distribution of MNs innervating a representative muscle in each group. Our results relating to all other muscles are presented as supplementary material. The functions of the individual muscle groups are

consistent with the descriptions in Sherrington (1910), Crouch (1969), and Vanderhorst and Holstege (1997).

2.1 Quadriceps group

This group contains the quadriceps femoris and the sartorius muscles. However, because the mouse sartorius is only present up to the thirteenth day of the embryonic life (Lance Jones 1979), our study concerned the MNs of the quadriceps femoris only. This muscle is mainly responsible for the extension of the knee. The four heads were injected simultaneously in each experiment.

2.1.1. Quadriceps femoris

The quadriceps MNs were arranged between L1 and L4, with the vast majority situated in L3. This MN column was the rostralmost of the hindlimb motor neuron groups in the lumbar cord. In transverse sections, the labeled cells occupied the ventromedial part of the ventral gray, ventral to the hamstring MN group. In rostral sections, the quadriceps MN group is located dorsomedial to the gluteal MN group, but more caudally it partially overlapped with that of the gluteal group (Fig. 4a1–a4).

2.2 Iliacus group

Muscles belonging to this group fix the vertebral column and flex the hip. Developmentally, the iliacus group consists of four muscles (psoas major, psoas minor, iliacus, and pectineus), but the pectineus is dealt with under heading 2.4.4.

2.2.1. Iliopsoas

The iliopsoas is formed by the psoas major and minor as well as the iliacus muscles. The caudal part of the iliopsoas was injected in three mice. Labeled MNs were localized in the most ventrolateral position of the ventral horn (Fig. 4b1–b4). Most FG-labeled cells were detected in L2–L3 but some were seen in L4, too.

2.3. Gluteal muscle group

According to their morphogenetic origin, the gluteal muscle group consists of seven muscles. (Lance Jones 1979). These muscles are responsible for the extension of the hip as well as for the abduction of the thigh. The two largest muscles belonging to this group (gluteus superficialis and gluteus medius) were injected in six mice.

2.3.1. Gluteus superficialis

The gluteus superficialis was injected in two EGFP-ChAT mice and one wild-type mouse. The labeled MNs were situated in the ventrolateral part of the ventral horn. The vast majority of the labeled cells were found in L4 and L5 but some MNs were also identified in L3 and L6 (Fig. 4c1–c4).

2.3.2. Gluteus medius

This muscle was injected in three mice. The rostrocaudal extent of the labeled neurons was similar to that of the gluteus superficialis MN group. FG-labeled cells were mostly detected in L4–L5 but some of them appeared in L3 and L6. MNs belonging to gluteus medius overlapped with those of the gluteus superficialis, forming a compact cell cluster within the boundaries of the gluteal MN group (see Online Resource 1).

2.4. Adductor group

Four muscles belonging to the adductor group were injected (namely, adductor magnus and longus, gracilis, and pectineus). Although the pectineus muscle belongs to the iliacus group on the basis of its morphogenetic origin (Lance Jones 1979), it is functionally more closely related to the adductor group. For this reason, we include the pectineus with the adductor group. The adductor MN group is located in the central cell column of the ventral horn.

2.4.1. Adductor magnus

The adductor magnus, the largest adductor, was injected in three mice. In two cases, the labeled MNs were detected from L2 to L5, inclusive. Within the boundaries of the adductor group, the cells belonging to the adductor magnus occupied the dorsomedial part but in more caudal segments they moved towards the ventral margin of the ventral horn (see Online Resource 2).

2.4.2. Adductor longus

Rostrocaudally, the extent of this MN group was almost the same as that of the adductor magnus MNs. The labeled MNs of adductor longus were detected between L2 and L5. In transverse sections, the labeled MNs were arranged in the medial part of the central cell column and overlapped with those of the adductor magnus (Fig. 5a1–a4).

2.4.3. Gracilis

In rodents, the gracilis possesses caudal and cranial heads. In the present experiments both heads were injected in each gracilis experiment (n = 3). The labeled cells extended from L3 to L5. When the position of the most rostral part of the gracilis MN group was compared with those of the adductor magnus and longus, the gracilis MNs were located more caudally. In

transverse sections, the gracilis MNs were seen in the dorsal part of the main motor nucleus (see Online Resource 3).

2.4.4. Pectineus

The pectineus was injected in five mice. As expected, the MNs of this most proximal adductor were located in the most rostral spinal segment. Generally, the labeled cells were detected in L2–L3 and only a few cells were located in either L1 or L4. The labeled MNs were found in the central cell column of the ventral gray matter (see Online Resource 4).

2.5. Hamstring group

The hamstring group contains five muscles (Lance Jones 1979) and they are responsible for the flexion of the knee and, to a lesser extent, for extension of the hip. The hamstring MN group is localized in the central column, showing a notable shift towards the ventral part of the ventral horn in its most caudal portion. Moreover, as previously described, hamstring MN columns showed partial overlap with the gluteal MN groups (McHanwell and Biscoe 1981a).

2.5.1. Biceps femoris

The biceps femoris was injected in six mice. The biceps femoris consists of two heads and is innervated by two nerves. The inferior gluteal nerve innervates the anterior head, while the main hamstring nerve innervates the posterior head (McHanwell and Biscoe 1981a). For this reason, the two heads were injected separately. After the FG injection into the anterior head, labeled MNs appeared between L4 and L6. In the case of the posterior head, labeled MNs were present from a more caudal level (L5). In transverse sections, the biceps MNs were situated in the ventral part of the central MN column. MNs associated with the posterior head were located dorsomedially to those of the anterior head (see Online Resource 5).

2.5.2. Semitendinosus

The semitendinosus muscle was injected in three mice. The semitendinosus has two heads, which were injected together in each case. Labeled MNs were located between L3 and L6. The semitendinosus MN group occupied the medial part of the hamstring group, overlapping with the semimembranosus MNs (see Online Resource 6).

2.5.3. Semimembranosus

This muscle was injected in three mice. The semimembranosus has two heads in mice (medial and lateral heads) and both of them were injected together in each case. The rostrocaudal extent of the labeled MNs overlapped with that of the semitendinosus, and the cells distributed evenly along the whole length of this MN column. The semimembranosus

MNs belong to the central MN column of the ventral horn, situating dorsomedial to the MN group innervating the anterior head of the biceps (Fig 5b1–b4).

2.6. Ischiotrochanteric group

This group is formed by four small muscles, which are located between the ischial border and the trochanteric region. In the present study, only the largest and most easily accessible member of the group (i.e., quadratus femoris) was injected. The quadratus femoris is responsible for the lateral rotation of the hip.

2.6.1. Quadratus femoris

Quadratus femoris MNs were seen mostly between L4 and L6, but in two mice a few labeled cells were also detected in L3. As seen in transverse sections, rostrally the quadratus femoris MN group occupies the medial division of the central column. Caudally, the quadratus MNs shift laterally and overlap with those of the gluteal MN group (Fig 5c1–c4).

2.7. Anterior crural group

The anterior crural group contains the tibialis anterior (in the superficial layer), which rotates the ankle joint outward, whereas muscles belonging to the deep layer of the anterior crural group are responsible for the extension of the digits.

2.7.1. Anterior crural superficial

MNs of the tibialis anterior muscle are located in L4–L5 and belong to the dorsolateral cell column. The labeled cells were adjacent to the lateral border of the posterior crural group (Fig 6a1–a3).

2.7.2. Anterior crural deep

In transverse sections, this MN group had the same position as that of the anterior crural superficial muscles but they extended more caudally, as far as rostral L6 (see Online Resource 7).

2.8. Lateral crural group

The lateral muscle compartment of the leg contains the peroneus longus and brevis, which are responsible for the dorsiflexion of the foot.

2.8.1. Peroneal muscles

Both peroneal muscles were injected together in each of three mice. Labeled cells were seen in the dorsolateral column of L4–L5. Mediolaterally, this cell group was situating along the lateral border of the gray matter and overlapped with the anterior crural MNs (Fig 6b1–b3).

2.9. Posterior crural group

Muscles belonging to this group are arranged in superficial and deep layers. All of them are flexors, acting on either the ankle or on the digits.

2.9.1 Posterior crural superficial

The superficial layer contains the triceps surae (consisting of the two heads of gastrocnemius, the soleus, as well as the plantaris muscle). The triceps surae is the main plantar flexor. All heads of the triceps surae were injected in every mouse (n = 3). The rostral part of the MN column was seen from L4, whereas its caudal end extended as far as L6. As Fig 6c1–c3 demonstrates, the labeled cells were arranged in the medial part of the dorsolateral column.

2.9.2. Posterior crural deep

This layer contains the long flexors of the foot and the tibialis posterior. After injecting these deep muscles, labeled cells were detected between L4 and L6. In transverse sections, the relevant MNs were found in the dorsolateral cell column, medial to the extensor MNs (see Online Resource 8).

2.10. Muscles of the foot

The muscles of the foot act as flexors, extensors, adductors, and abductors of the digits.

2.10.1. Extensor digitorum brevis

Although the extensor digitorum brevis is located on the dorsal surface of the foot, it is not an ‘intrinsic’ foot muscle. Rather, it belongs developmentally to the crural extensor muscle group. After injecting the extensor digitorum brevis, the majority of the FG-labeled MNs were seen in L6, although a few MNs were also detected in L5. MNs innervating the extensor digitorum brevis belong to the dorsolateral cell column (see Online Resource 9).

2.10.2. Plantar muscles

The majority of the labeled MNs appeared in L6 but some cells were detected in L5. In transverse sections, plantar MNs were scattered in the dorsolateral cell column (Fig 6d1–d3).

Discussion

1. Methodological considerations relating to retrograde tracing

MNs are essential but vulnerable parts of the motor system. Damage to these neurons has a huge impact on quality of life. It should not be surprising, therefore, that investigation of the distribution of MNs innervating individual limb muscles has attracted much attention in the past. Precise knowledge regarding the topography of MNs has clinical relevance, especially with the advent of animal models resembling human ALS.

The pioneering studies of Waldeyer (1888), Kaiser (1891), and Romanes (1941, 1951, 1964) revealed the basic principles of organization of spinal MNs. However, as Routal and Pal (1999) pointed out about a century later, unless retrograde tracing is applied, defining the territories of the MN groups is very difficult. Most importantly, the individual MN groups have imperfect boundaries. Furthermore, the size and shape of these clusters are highly variable, resulting in marked differences which are not only present when closely related species are considered (e.g., rats and mice) but they are evident within the same species or even when the two sides of the same spinal section are compared. Early studies without the benefit of modern retrograde tracing methods were handicapped in their efforts to define the relationships between muscle groups and motor neuron clusters (Romanes, 1951).

When horseradish peroxidase (HRP) retrograde labeling became a standard technique, most of these difficulties could be effectively dealt with, yielding some very careful and detailed mapping of mammalian hindlimb MN groups (McHanwell and Biscoe 1981a,b; Nicolopoulos-Stournaras and Iles 1983, Vanderhorst and Holstege 1997). These studies are benchmarks in the field of MN labeling, so that one might reasonably ask whether additional studies regarding hindlimb MN groups are justified. The comprehensive nature of these studies may be one reason why relatively few articles have been published on this subject in recent times. Recent articles are mostly focused on a limited number of muscles, often in association with ALS (e.g., Mohajeri et al. 1998).

Nevertheless, thematic studies aimed at mapping and quantification of MN groups innervating forelimb and hindlimb muscles are still timely and important. Most importantly, very little information is available on mice of the C57BL/6J strain, which is the strain on which most transgenic lines are based. Interspecies comparisons are limited in value and variability exists even within the same strain (Rigaud et al., 2008). Ideally, researchers should have access to detailed data from the relevant strain to have a comprehensive understanding of the actual size and distribution of the various MN groups. This is especially true for the

quantitative data, which have specific relevance when characterizing the progression of MN loss and efficacy of treatment strategies in animal models of ALS.

In the present work, we chose FG as a retrograde tracer because it offers some clear advantages (Schmued and Fallon 1986; Mohajeri et al. 1998). FG is not degraded by lysosomes, thus it provides strong labeling that remains visible for a long period of time (up to one year). FG injection does not affect the function of the labeled muscles. Additionally, FG is a fluorescent dye and can therefore be visualized using conventional fluorescence or confocal microscopy. These techniques permit acquisition of high quality images and also allow the application of advanced image processing, including 3D reconstruction. Although this approach has been already successfully utilized by Yan et al. (2007) for the description of the spatial distribution of MNs innervating the rat trapezius muscle, the method has not hitherto been extended to muscle groups innervating an entire limb. Although there have been reports indicating that FG may have detrimental effects on the labeled neurons (e.g., Garrett et al. 1991; Franklin and Druhan 2000; Naumann et al. 2000), other studies did not observe neurotoxic effects associated with FG application (e.g., Emsley et al. 2001; McClellan et al. 2006). Because the situation is not yet clear, the possibility of adverse effect must be borne in mind when using FG tracing.

Despite well-regarded earlier attempts to map and characterize MN groups innervating individual muscles of the mammalian hindlimb, we believe that our study is particularly relevant for a number of reasons. Firstly, the present study was conducted on mice belonging to the C57BL strain, whereas the study of McHanwell and Biscoe (1981a) was conducted on C129ReJ mice; our results can therefore be directly applied to describe the MN loss in transgenic ALS models based on the C57BL strain. Secondly, the green fluorescence of the MNs allowed easy and reliable comparison of the positions of the FG-labeled (yellow) and non-labeled (green) MN groups in the same spinal section. Thirdly, the application of FG allowed reliable and easily detectable labeling of the individual MN groups. Fourthly, FG is less prone to spreading, thus inadvertent labeling of non-innervating MNs was less likely than with the application of HRP. Finally, for the first time in the literature, we have developed a 3D model to provide a better understanding of the spatial distribution of the labeled hindlimb MN groups.

2. A difference between C57BL and C129ReJ mice

When comparing our results on C57BL mice with those of McHanwell and Biscoe (1981a) on C129ReJ mice, we noticed an important difference in the segmental level supplying the

intrinsic muscles of the foot. In the C57BL mice these MNs were located in the L6 segment, whereas in C129ReJ mice they were identified by McHanwell and Biscoe (1981a) as lying in the L5 segment. This interesting strain difference indicates that the hindlimb enlargement of the cord in the C129ReJ mouse is prefixed by one segment compared to the C57BL mouse. Interstrain differences such as this have been previously reported and occasionally such variation occurs among members of the same strain (Rigaud et al., 2008).

3. Motoneuron columns in the ventral horn

Since the careful study of Romanes (1951), it has been known that limb MNs form three distinct longitudinal columns in the ventral horn. Although the rostrocaudal extent of these columns shows interspecies variability (see Table 3 for details), their relative positions are consistent in studies of rat, mouse, and cat (McHanwell and Biscoe 1981a,b; Nicolopoulos-Stournaras and Iles 1983, Vanderhorst and Holstege 1997). In our work, we also identified these cell columns (Fig. 7).

Ventrolateral (VL) cell column: The VL cell column appears in the rostralmost position of the ventrolateral part of the lumbar gray matter. At the level of L1, the VL column begins with MNs innervating the quadriceps femoris. Inside the cell column, the quadriceps MNs occupy the dorsomedial part and remain in this position as far as L4. At the level of L2, the iliopsoas MNs form the most lateral part of the VL column. More caudally (L3), the gluteal MNs join this column, situating between the iliopsoas and quadriceps MNs, and ventral to the quadriceps group.

Dorsolateral (DL) cell column: The DL column extends from L4 to L6 and accommodates MNs innervating the muscles of the crural region and the intrinsic musculature of the foot. The most lateral part of this column is occupied by MNs belonging to the lateral crural muscles, whereas the ventromedial part of the DL column is formed by MNs of the anterior crural muscles. These two muscle groups are innervated by branches of the common peroneal nerve. In our study, the lateral crural MN group (related to muscles supplied by the superficial peroneal nerve) terminated more rostrally (L5), whereas the anterior crural MN group could be followed as far as L6. In previous studies on mice and rats, the lateral crural MNs were reported to extend somewhat more caudally (e.g., McHanwell and Biscoe 1981a, Nicolopoulos-Stournas and Iles 1983). The explanation for this difference is not certain, although the possible variability of the actual extent of the individual MN groups, as well as differences in the applied techniques may contribute to the different observations. The medial part of the DL cell column is formed by MNs innervating

the posterior crural muscles, while the dorsal-most area of the DL cell column contains MNs supplying the intrinsic musculature of the foot.

Central cell column: The central cell column is located in the middle of the ventral horn, extending from L2 to L6. Its rostral part is formed by MNs of the adductor muscles. Rostrally, this MN column is seen in a dorsolateral position, but it shifts medially and ventrally as it approaches more caudal spinal segments (e.g., L5). At the level of L3, some hamstring MNs (i.e., those supplying the semimembranosus and semitendinosus) join the medial part of the adductor MN column. More caudally, the hamstring MN group, along with the entire central cell column, shifts towards a more ventromedial position and terminates in L6. The third MN group of the central column innervates the quadratus femoris, which is a member of the ischiotrochanteric group. The relevant MNs appear in L3 and occupy the most ventral and medial position of the central group. The quadratus femoris cell group extends to L6 and shifts dorsomedially within the central MN column.

4. Somatotopic organization of the MNs in the ventral horn

The MNs groups are arranged to form longitudinal cell columns and they show a conserved organization when viewed in transverse sections of the spinal cord. This arrangement of the individual MN groups is related to the ontogenetic origin, localization, and function of the innervated muscles (Lance Jones 1979; Ryan et al. 1998).

First, as it has been noted previously (Lance Jones 1979), the muscles of the lower limb can be grouped on the basis of their ontogenetic origin. MNs pools innervating these groups are arranged mediolaterally in the ventral horn. MNs belonging to muscles that develop from the dorsal muscle mass (e.g., quadriceps femoris and gluteal muscles) are situated in the lateral part of the ventral gray. In contrast, MNs innervating muscles originating from the ventral muscle mass (e.g., adductors, hamstring, and ischiotrochanteric muscles) occupy the medial part of the ventral horn.

Second, MN pools also show a dorsoventral distribution, based on the position of the supported muscle relative to the pelvis; MNs supplying proximal muscles are present more ventrally. In our study, MNs innervating muscles of the hip joint (e.g., iliopsoas, gluteal, and quadratus femoris) occupied the ventralmost position, whereas MNs of the dorsalmost cell group supplied the most distal muscles of the hindlimb — the intrinsic musculature of the foot. The MNs that innervate muscles of the knee (i.e., adductors, hamstring, and quadriceps) and the ankle joints (i.e., anterior, lateral, and posterior crural muscles) were situated between those of the hip and the foot. It should be noted that the localization of the muscles did not

only correlate with the dorsoventral positions of the MNs but with their rostrocaudal arrangement as well. The rostrocaudal position of each MN group also reflects the proximo-distal localization of the innervated muscles. For example, MNs innervating the iliopsoas (the most proximally located muscle in our experiments) were located between L2 and L4, whereas MNs belonging to the more distal quadratus femoris appeared in L3–L6 segments. Similarly, MNs of the more proximal lateral crural muscle were seen more rostrally (L4–L5) than those of the most distally located plantar muscles (L5–L6).

Third, MNs are also arranged according to the function of the muscles they innervate. Similar to the situation noted in the upper limb (Bácskai et al. 2012), the clusters of flexor and extensor MNs showed a mediolateral orientation. MNs belonging to the posterior crural muscles, the main flexors of the ankle joint, were situated more medially than those of the anterior crural muscles (i.e., the extensors of the ankle). MNs innervating the flexors (i.e., hamstring muscles) and the extensors (i.e., quadriceps femoris) of the knee joint show a similar pattern of organization.

5. The iliopsoas problem

There have been only a few attempts to localize the MN groups associated with the iliopsoas and the results are difficult to interpret. In their study on rats, Nicolopoulos-Stournas and Iles (1983) labeled the iliacus motor neurons only. They found the iliacus MN column to lie in the middle part of the ventral horn, adjacent to the white matter, and medial to that of the pectineus. Vanderhorst and Holstege (1997) injected the entire distal part of the cat iliopsoas with retrograde tracer and the labeled motor neurons were in two distinct groups: one was in the ventrolateral corner of the ventral horn, and another in the medial part of the ventral horn, near the white matter. Selective targeting of the psoas revealed the ventrolateral MN group only. The mouse spinal cord atlas (Watson et al. 2009a*)* represents the psoas MN group in the medial part of the ventral horn, close to the position of the putative iliacus MN column in the cat (Vanderhorst and Holstege, 1997). In our present work, after injecting the distal part of the iliopsoas, only one MN group was seen, which was situated in the ventrolateral corner of the ventral horn (Fig. 4b1–b4). This position is identical to that associated with the position of the psoas MNs in the cat (Vanderhorst and Holstege, 1997).

Additionally, the iliopsoas MN group does not appear to obey some of the organization rules explained previously. It is known that MNs innervating muscles developing from the ventral and dorsal muscle masses are preferentially localized to the medial and lateral parts of the ventral gray, respectively. However, as the iliopsoas develops

from both muscle masses (Lance Jones 1979), this rule of organization is not applicable. Moreover, iliopsoas MNs seem to breach the rule governing the relative positions of flexors and extensors. The iliopsoas muscle is a major flexor of the hip, thus its MNs would be expected more medial than those of the hip extensors (i.e., the gluteal group). However, in two most relevant studies (Nicolopoulos-Stournas and Iles 1983; Vanderhorst and Holstege 1997), and in the present one, the gluteal and iliopsoas MN groups appear to occupy very similar positions.

6. Relevance of the present findings to ALS research

The present results are relevant to ALS research. ALS is one of the most devastating neurological diseases (e.g., Boillée et al. 2006), progressing rapidly and affecting both motor neurons (Hanyu et al. 1982) and long spinal tracts (Sobue et al. 1987). In the past years, over 500 products and several treatment strategies have been investigated (e.g. Miller et al. 2005; Nagano et al. 2005a,b; Ralph et al. 2005; Chi et al. 2006; de Hemptinne et al. 2006; Traynor et al. 2006; Orrell, 2010) with rather limited success even in the most promising cases (e.g., Bensimon et al. 1994; Azzouz et al. 2004; Bachurin et al. 2011, or Cudkowicz et al. 2011). It is clear that objective assessment of efforts aimed at finding suitable ALS therapies would be assisted by extensive testing on suitable animal models, thorough scrutiny of the results with methods that permit monitoring of the progression of the disease, and quantitative analysis of the neuronal loss associated with ALS. It has been suggested that methodological problems associated with preclinical trials performed on mouse models might be behind the lack of translation of therapies from animal models to patients (Joyce et al. 2011). It follows that there is a strong need to have objective and easily quantifiable data that would assist ALS research. The data presented in this study and in our study of forelimb muscles (Bácskai et al., 2012), along with those demonstrated in some earlier efforts (e.g., McHanwell and Biscoe 1981a,b; Watson et al. 1982; Ashwell and Watson 1983; Watson et al. 2009a,b; McHanwell and Watson 2009) are useful in this regard for a number of reasons.

First, establishing and comparing the number of MNs innervating individual muscles in control and $SOD1^{G93A}$ mice may provide information about the onset, progression, and severity of the MN loss.

Secondly, it has been noted that in the earliest phase of ALS, the motor neuron terminals are withdrawn from the innervated skeletal muscle fibers resulting in the discontinuation of the motor neuron-skeletal muscle contact (Kong and Xu 1998; Frey et al. 2000; Fischer et al. 2004; Pun et al. 2006). Since this phase is not accompanied by neural

degeneration or clinical symptoms, the only way to identify this stage is to recognize the reduction of the number of available neuromuscular junctions. Because labeling of the motor neurons after intramuscular injection of the retrograde tracer requires intact neuromuscular junctions, this method can give indication of the onset and early progression of the disease, even in the absence of clinical symptoms or without signs of muscular atrophy. However, to detect reduction of the labeled motor neuron numbers in animal models of ALS, age-matched canonical values are needed — such as those provided by our present and preceding work (Bácskai et al. 2012).

Thirdly, it would be useful to gain detailed information about the distribution of muscle groups that are more prone to motor neuron loss in ALS. MNs innervating fast-fatigable skeletal muscle fibers are more prone to neuronal damage associated with ALS than fast–fatigue-resistant (showing intermediate susceptibility), or slow fibers (Frey et al., 2000; Pun et al, 2006). It follows that muscles containing high proportion of slow fibers (e.g., soleus) are expected to be affected less severely than those having a higher proportion of fast-fatigable fibers (e.g., biceps). However, these trends cannot be confirmed unless reliable information is available about the number of MNs innervating the relevant muscles in control mice.

Finally, although functional studies are important for assessing the onset, course, and severity of ALS as well as for determining the effects of new treatment strategies, these studies are often difficult to quantify and compare objectively. Our present results provide objective data to describe the number of MNs in control mice, which could assist research efforts aimed at MN investigation in general and at ALS research in particular.

Acknowledgements

This study was supported by an NHMRC (National Health & Medical Research Council) Australia Fellowship Grant awarded to Dr George Paxinos (Grant #568605).

The authors declare that they have no conflict of interest.

References

Abercrombie M (1946) Estimation of nuclear population from microtome sections. Anat Rec 94:239–247

Ashwell KW, Watson CRR (1983) The development of facial motoneurones in the mouse — neuronal death and the innervation of the facial muscles. J Embryol Exp Morphol 77:117-141

Azzouz M, Ralph GS, Storkebaum E, Walmsley LE, Mitrophanous KA, Kingsman SM, Carmeliet P, Mazarakis ND (2004) VEGF delivery with retrogradely transported lentivector prolongs survival in a mouse ALS model. Nature 429:413–417

Bachurin SO, Shelkovnikova TA, Ustyugov AA, Peters O, Khritankova I, Afanasieva MA, Tarasova TV, Alentov II, Buchman VL, Ninkina NN (2011) Dimebon slows progression of proteinopathy in γ-synuclein transgenic mice. Neurotox Res 22:33–42

Bácskai T, Fu Y, Sengul G, Rusznák Z, Paxinos G, Watson C (2012) Musculotopic organization of the motor neurons supplying forelimb and shoulder girdle muscles in the mouse. Brain Struct Funct (Epub, ahead of print)

Beckman JS, Carson M, Smith CD, Koppenol WH (1993) ALS, SOD and peroxynitrite. Nature 364:584–584

Bensimon G, Lacomblez L, Meininger V, and the ALS/Riluzole Study Group (1994) A controlled trial of riluzole in amyotrophic lateral sclerosis. N Engl J Med 330:585–591

Boillée S, Vande Velde C, Cleveland DW (2006) ALS: a disease of motor neurons and their nonneuronal neighbors. Neuron 52:39–59

Chi L, Ke Y, Luo C, Li B, Gozal D, Kalyanaraman B, Liu R (2006) Motor neuron degeneration promotes neural progenitor cell proliferation, migration, and neurogenesis in the spinal cords of amyotrophic lateral sclerosis mice. Stem Cells 24: 34–43

Crouch JE (1969) Text-Atlas of cat anatomy. Lea and Febiger, Philadelphia

Cudkowicz M, Bozik ME, Ingersoll EW, Miller R, Mitsumoto H, Shefner J, Moore DH, Schoenfeld D, Mather JL, Archibald D, Sullivan M, Amburgey C, Moritz J, Gribkoff VK (2011) The effects of dexpramipexole (KNS-760704) in individuals with amyotrophic lateral sclerosis. Nat Med 17:1652–1656

de Hemptinne I, Boucherie C, Pochet R, Bantubungi K, Schiffmann SN, Maloteaux JM, Hermans E (2006) Unilateral induction of progenitors in the spinal cord of hSOD1(G93A) transgenic rats correlates with an asymmetrical hind limb paralysis. Neurosci Lett 401:25–29

Emsley JG, Lu X, Hagg T (2001) Retrograde tracing techniques influence reported cell death rates of adult rat nigrostriatial neurons. Exp Neurol 168:425–433

Fischer LR, Culver DG, Tennant P, Davis AA, Wang M, Castellano-Sanchez A, Khan J, Polak MA, Glass JD (2004) Amyotrophic lateral sclerosis is a distal axonopathy: evidence in mice and man. Exp Neurol 185:232–240

Franklin TR, Druhan JP (2000) The retrograde tracer fluoro-gold interferes with the expression of fos-related antigens. J Neurosci Methods 98:1–8

Frey D, Schneider C, Xu L, Borg J, Spooren W, Caroni P (2000) Early and selective loss of neuromuscular synapse subtypes with low sprouting competence in motoneuron diseases. J Neurosci 20:2534–2542

Garrett WT, McBride RL, Williams JK, Feringa ER (1991) Fluoro-Gold's toxicity makes it inferior to True Blue for long-term studies of dorsal root ganglion neurons and motoneurons, Neurosci Lett 128:137–139

Green EC (1959) Anatomy of the rat. Hafner, New York

Gurney, M.E., Pu, H., Chiu, A.Y., Dal Canto, M.C., Polchow, C.Y., Alexander, D.D., Caliendo, J., Hentati, A., Kwon, Y.W., Deng, H.X., Zhai, P., Sufit, R.L., Siddique, T. (1994) Motor neuron degeneration in mice that express a human Cu,Zn superoxide dismutase mutation. Science 264:1772–1775.

Haenggeli C, Kato AC (2002) Rapid and reproducible methods using fluorogold for labelling a subpopulation of cervical motoneurons: application in the wobbler mouse. J Neurosci Methods 116:119–124

Hanyu N, Oguchi K, Yanagisawa N, Tsukagoshi H (1982) Degeneration and regeneration of ventral root motor fibers in amyotrophic lateral sclerosis. Morphometric studies of cervical ventral roots. J Neurol Sci 55:99–115

Hebel R, Stromberg MW (1976) Anatomy of the laboratory rat. Williams &Wilkins, Baltimore

Joyce PI, Fratta P, Fisher EMC, Acevedo-Arozena A (2011) SOD1 and TDP-43 animal models of amyotrophic lateral sclerosis: recent advances in understanding disease toward the development of clinical treatments. Mamm Genome 22:420–448

Kaiser O (1891) Die Functionen der Ganglienzellen des Halsmarkes. Haag.

Kong J, Xu Z (1998) Massive mitochondrial degeneration in motor neurons triggers the onset of amyotrophic lateral sclerosis in mice expressing a mutant SOD1. J Neurosci 18:3241–3250

Kwiatkowski TJ Jr, Bosco DA, Leclerc AL, Tamrazian E, Vanderburg CR, Russ C, Davis A, Gilchrist J, Kasarskis EJ, Munsat T, Valdmanis P, Rouleau GA, Hosler BA, Cortelli P, de Jong PJ, Yoshinaga Y, Haines JL, Pericak-Vance MA, Yan J, Ticozzi N, Siddique T, McKenna-Yasek D, Sapp PC, Horvitz HR, Landers JE, Brown RH Jr (2009) Mutations in the FUS/TLS gene on chromosome 16 cause familial amyotrophic lateral sclerosis. Science 27:1205–1208

Lance Jones C (1979) The morphogenesis of the thigh of the mouse with special reference to tetrapod muscle homologies. J Morphol 162:275–310

Mackenzie IR, Rademakers R, Neumann M (2010) TDP-43 and FUS in amyotrophic lateral sclerosis and frontotemporal dementia. Lancet Neurol 9:995–1007

McClellan AD, Zhang L, Palmer R (2006) Flurogold labeling of descending brain neurons in larval lamprey does not cause cell death. Neurosci Lett 401:119–124

McHanwell S, Biscoe TJ (1981a) The localization of motor neurons supplying the hindlimb muscles of the mouse. Philos Trans R Soc Lond B Biol Sci 293:477–508

McHanwell S, Biscoe TJ (1981b) The sizes of motoneurons supplying hindlimb muscles in the mouse. Proc R Soc Lond B 213:201–216

McHanwell S, Watson C (2009) Localization of motoneurons in the spinal cord. In: Watson C, Paxinos G, Kayalioglu G (eds) Spinal Cord. A Christopher and Dana Reeve Foundation Text and Atlas, Elsevier, San Diego, pp. 94–114

McLaren A, Michie D (1954) Factors affecting vertebral variation in mice. 1. Variation within an inbred strain. J Embryol exp Morph 2:149–160

McLaren A, Michie D (1958) Factors affecting vertebral variation in mice. 4. Experimental proof of the uterine basis of a maternal effect. J Embryol exp Morph 6:645–659

Miller TM, Kaspar BK, Kops GJ, Yamanaka K, Christian LJ, Gage FH, Cleveland DW (2005) Virus-delivered small RNA silencing sustains strength in amyotrophic lateral sclerosis. Ann Neurol 57:773–776

Mohajeri MH, Figlewicz DA, Bohn MC (1998) Selective loss of α motoneurons innervating the medial gastrocnemium muscle in a mouse model of amyotrophic lateral sclerosis. Exp Neurol 150:329–336

Nagano I, Ilieva H, Shiote M, Murakami T, Yokoyama M, Shoji M, Abe K (2005a) Therapeutic benefit of intrathecal injection of insulin-like growth factor-1 in a mouse model of amyotrophic lateral sclerosis. J Neurol Sci 235:61–68

Nagano I, Shiote M, Murakami T, Kamada H, Hamakawa Y, Matsubara E, Yokoyama M, Moritaz K, Shoji M, Abe K (2005b) Beneficial effects of intrathecal IGF-1 administration in patients with amyotrophic lateral sclerosis. Neurol Res 27:768–772

Naumann T, Härtig W, Frotscher M (2000) Retrograde tracing with Fluoro-Gold: different methods of tracer detection at the ultrastructural level and neurodegenerative changes of back-filled neurons in long-term studies. J Neurosci Methods 103:11–21

Nicolopoulos-Stournas S, Iles JF (1983) Motor neuron columns in the lumbar spinal cord of the rat. J Comp Neurol 217:27–85

Orrell RW (2010). Motor neuron disease: systematic reviews of treatment for ALS and SMA. Br Med Bull 93:145–159

Pun S, Santos AF, Saxena S, Xu L, Caroni P (2006) Selective vulnerability and pruning of phasic motoneuron axons in motoneuron disease alleviated by CNTF. Nat Neurosci 9:408–419

Portal JJ, Corio M, Viala D (1991) Localization of the lumbar pools of motoneurones which provide hindlimb muscles in the rabbit Neurosci Lett, 124:105–107

Ralph GS, Radcliffe PA, Day DM, Carthy JM, Leroux, MA, Lee DC, Wong LF, Bilsland LG, Greensmith L, Kingsman SM, Mitrophanous KA, Mazarakis ND, Azzouz M (2005) Silencing mutant SOD1 using RNAi protects against neurodegeneration and extends survival in an ALS model. Nat Med 11:429–433

Rigaud M, Gemes G, Barabas ME, Chernoff DI, Abram SE, Stucky CL, Hogan, QH. (2008) Species and strain differences in rodent sciatic nerve anatomy: implications for studies of neuropathic pain. Pain 136:188-201.

Romanes GJ (1941) The development and significance of the cell columns in the ventral horn of the cervical and upper thoracic spinal cord of the rabbit. J Anat 76:112–130

Romanes GJ (1951) The motor cell columns of the lumbosacral spinal cord of the cat. J Comp Neurol 94:313–363

Romanes, GJ (1964) The motor pools of the spinal cord. Progr Brain Res 11:93–119

Routal RV, Pal GP (1999) A study of motoneurone groups and motor columns of the human spinal cord. J Anat 195:211–234

Ryan JM, Cushman J, Jordan B, Samuels A, Frazer H, Baier C (1998) Topographic position of forelimb motoneuron pools is conserved in vertebrate evolution. Brain Behav Evol 51:90–99

Sasabe J, Miyoshib Y, Suzuki M, Mita M, Konno R, Matsuoka M, Hamase K, Aiso S (2012) D-Amino acid oxidase controls motoneuron degeneration through D-serine. Proc Natl Acad Sci USA 109:627–632

Schmued LC, Fallon JH (1986) Fluoro-Gold: a new fluorescent retrograde axonal tracer with numerous unique properties. Brain Res 377:147–154

Sengul G, Tanaka I, Paxinos G, Watson C (2012) Atlas of spinal cords of the rat, mouse, marmoset, macaque, and human. Elsevier Academic Press, San Diego (in press)

Sherrington CS (1910) Flexion-reflex of the limb, crossed extension-reflex, and reflex stepping and standing. J Physiol 40:28–121

Sobue G, Hashizume Y, Mitsuma T, Takahashi A (1987) Size-dependent myelinated fiber loss in the corticospinal tract in Shy-Drager syndrome and amyotrophic lateral sclerosis. Neurology 37:529–532

Traynor BJ, Brujin L, Conwit R, Beal F, O'Neill G, Fagan SC, Cudkowicz ME (2006) Neuroprotective agents for clinical trials in ALS: a systematic assessment. Neurology 67:20–27

Vanderhorst VGJM, Holstege G (1997) Organization of lumbosacral motoneuronal cell groups innervating hindlimb, pelvic floor, and axial muscles in the cat. J Comp Neurol 382:46–76

Waldeyer W (1888) Das Gorilla-Rückenmark. Abh der Königlichen Akad der Wissensch Berlin Phys-Math Classe, Abh III, pp 1–147

Watson CRR, Sakai S, Armstrong W (1982) The organization of the facial nucleus in the rat. Brain Behav and Evol 20:19–28

Watson C, Paxinos G, Kayalioglu G, Heise C (2009a) Atlas of the mouse spinal cord. In: Watson C, Paxinos G, Kayalioglu G (eds) Spinal Cord. A Christopher and Dana Reeve Foundation Text and Atlas, Elsevier, San Diego, pp. 308–379

Watson C, Paxinos G, Kayalioglu G, Heise C (2009b) Atlas of the rat spinal cord. In: Watson C, Paxinos G, Kayalioglu G (eds) Spinal Cord. A Christopher and Dana Reeve Foundation Text and Atlas, Elsevier, San Diego, pp. 238–306

Wiedau-Pazos M, Goto JJ, Rabizadeh S, Gralla EB, Roe, JA, Lee MK, Valentine JS, Bredesen DE (1996) Altered reactivity of superoxide dismutase in familial amyotrophic lateral sclerosis. Science 271:515–518

Yan J, Aizawa Y, Hitomi J (2007) Localization of motoneurons that extend axons through the ventral rami of cervical nerves to innervate the trapezius muscle: a study using fluorescent dyes and 3D reconstruction method. Clin Anat 20:41–47

Figure legends

Figure 1

Demonstration of the results of good and technically inappropriate iliopsoas injections. (a) Image taken after muscle injection when the tracer did not fill the muscle completely. Only few, faintly labeled motor neurons are visible. (b) Result of a good muscle injection. The labeled motor neurons appear in the expected territory of the iliopas motor nucleus, forming a tight cluster of cells. (c) Extensive leakage of FG. Labeled motor neurons are not confined to the expected territory of the iliopsas motor nucleus but they are present in adjacent regions, including the putative motor nucleus of the quadriceps muscle. Labelings exemplified in (a) (c) were not taken into consideration during the analysis but the relevant experiments were repeated. Each image was taken from different mice at the level of L3. Scale bar: 200 μm.

Figure 2

ChAT-EGFP expression from L1 to L6. The cholinergic MNs are visible as green profiles in the ventral horn. The putative borders of the individual MN groups are also indicated. MN groups indicated by asterisk could not be unambiguously associated with any muscle or muscle group. Scale bar: 200 μm.

Figure 3

High magnification images demonstrating FG-labeled MNs in the lumbar spinal cord. (a–b) Putative α-motor neurons. (c–d) Putative γ-motor neurons. Scale bar: 20 μm.

Figure 4

Extent and organization of MN groups innervating the quadriceps femoris, iliopsoas, and gluteus superficialis muscles. (a1–a3) Photomicrographs of transverse sections from different levels of the spinal cord (as indicated in the bottom-right corner) after FG injections into the quadriceps femoris. The inset in (a2) depicts the topography of the MN columns as demarcated in transverse sections prepared from a ChAT-EGFP mouse. The MN group with the framed abbreviation corresponds to that revealed by retrograde labeling. (a4) 3D reconstruction of the number and distribution of MNs innervating the quadriceps femoris. Gray lines mark the border of the gray matter, green circles represent the central canal, and each red dot corresponds to the cell body of a single MN. White (rostralmost), blue, and yellow (caudalmost) arrows indicate the positions where the photomicrographs were taken.

(b1–b4) Number and distribution of MNs innervating the iliopsoas. The organization of the panels is the same as in (a1–a4). (c1–c4) Number and distribution of MNs innervating the gluteus superficialis. The organization of the panels is the same as in (a1–a4). D: dorsal, C: caudal, L: lateral, and M: medial. Scale bars: 200 µm.

Figure 5

Extent and organization of MN groups innervating the adductor longus, semimembranosus, and quadratus femoris. (a1–a4) Number and distribution of MNs innervating the adductor longus. (b1–b4) Number and distribution of MNs innervating the semimembranosus. (c1–c4) Number and distribution of MNs innervating the quadratus femoris. The organization of the panels is the same as in Figure 3. D: dorsal, C: caudal, L: lateral, and M: medial. Scale bars: 200 µm.

Figure 6

Extent and organization of MN groups innervating the anterior crural superficial, lateral crural, posterior crural superficial, and plantar foot muscles. (a1–a3) Number and distribution of MNs innervating the anterior crural superficial muscles. (b1–b3) Number and distribution of MNs innervating the lateral crural muscles. (c1–c3) Number and distribution of MNs innervating the posterior crural superficial muscles. (d1–d3) Number and distribution of MNs innervating the plantar foot muscles. The organization of the panels is the same as in Figure 3. D: dorsal, C: caudal, L: lateral, and M: medial. Scale bars: 200 µm.

Figure 7

A synopsis of the data demonstrating the rostrocaudal extents and organization of MN columns innervating the major muscles of the mouse hindlimb. The borders of the individual spinal cord segments are indicated. Gray columns with black borders demonstrate the extent of MN groups as presented in the mouse spinal cord atlas (Watson et al. 2009a). In the case of the iliopsoas, only the psoas MN group is depicted in the atlas, extending from L2 to L3.

Legends to the supplementary material

Online Resource 1

Extent and organization of the MN group innervating the gluteus medius. (a1–a3) Photomicrographs of transverse sections from different levels of the spinal cord (as indicated in the bottom-right corner) after FG injections. (a4) 3D reconstruction of the number and distribution of MNs innervating the gluteus medius. Gray lines mark the border of the gray matter, green circles represent the central canal, and each red dot corresponds to the cell body of a single MN. White (rostralmost), blue, and yellow (caudalmost) arrows indicate the positions where the photomicrographs were taken. D: dorsal, C: caudal, and L: lateral. Scale bar: 200 μm.

Online Resource 2

Extent and organization of the MN group innervating the adductor magnus. (a1–a3) Photomicrographs of transverse sections from different levels of the spinal cord (as indicated in the bottom-right corner) after FG injections. (a4) 3D reconstruction of the number and distribution of MNs innervating the adductor magnus. Gray lines mark the border of the gray matter, green circles represent the central canal, and each red dot corresponds to the cell body of a single MN. White (rostralmost), blue, and yellow (caudalmost) arrows indicate the positions where the photomicrographs were taken. D: dorsal, C: caudal, and M: medial. Scale bar: 200 μm.

Online Resource 3

Extent and organization of the MN group innervating the gracilis. (a1–a3) Photomicrographs of transverse sections from different levels of the spinal cord (as indicated in the bottom-right corner) after FG injections. (a4) 3D reconstruction of the number and distribution of MNs innervating the gracilis. Gray lines mark the border of the gray matter, green circles represent the central canal, and each red dot corresponds to the cell body of a single MN. White (rostralmost), blue, and yellow (caudalmost) arrows indicate the positions where the photomicrographs were taken. D: dorsal, C: caudal, and M: medial. Scale bar: 200 μm.

Online Resource 4

Extent and organization of the MN group innervating the pectineus. (a1–a2) Photomicrographs of transverse sections from different levels of the spinal cord (as indicated

in the bottom-right corner) after FG injections. (a3) 3D reconstruction of the number and distribution of MNs innervating the pectineus. Gray lines mark the border of the gray matter, green circles represent the central canal, and each red dot corresponds to the cell body of a single MN. White (rostral) and yellow (caudal) arrows indicate the positions where the photomicrographs were taken. D: dorsal, C: caudal, and M: medial. Scale bar: 200 μm.

Online Resource 5

Extent and organization of MN groups innervating the biceps femoris. (a1–a3) Photomicrographs of transverse sections from different levels of the spinal cord (as indicated in the bottom-right corner) after FG injections into the anterior head of biceps femoris muscle. (b1–b2) Photomicrographs of transverse sections from different levels of the spinal cord (as indicated in the bottom-right corner) after FG injections into the posterior head of biceps femoris. (c1–c2) 3D reconstruction of the number and distribution of MNs innervating the anterior and posterior heads. Gray lines mark the border of the gray matter, green circles represent the central canal, and each red dot corresponds to the cell body of a single MN. White (rostralmost), blue, and yellow (caudalmost) arrows indicate the positions where the photomicrographs were taken. D: dorsal, C: caudal, and M: medial. Scale bars: 200 μm.

Online Resource 6

Extent and organization of the MN group innervating the semitendinosus. (a1–a3) Photomicrographs of transverse sections from different levels of the spinal cord (as indicated in the bottom-right corner) after FG injections. (a4) 3D reconstruction of the number and distribution of MNs innervating the semitendinosus. Gray lines mark the border of the gray matter, green circles represent the central canal, and each red dot corresponds to the cell body of a single MN. White (rostralmost), blue, and yellow (caudalmost) arrows indicate the positions where the photomicrographs were taken. D: dorsal, C: caudal, and M: medial. Scale bar: 200 μm.

Online Resource 7

Extent and organization of the MN group innervating the deep anterior crural muscles. (a1–a3) Photomicrographs of transverse sections from different levels of the spinal cord (as indicated in the bottom-right corner) after FG injections. (a4) 3D reconstruction of the number and distribution of MNs innervating the deep anterior crural muscles. Gray lines mark the border of the gray matter, green circles represent the central canal, and each red dot

corresponds to the cell body of a single MN. White (rostralmost), blue, and yellow (caudalmost) arrows indicate the positions where the photomicrographs were taken. D: dorsal, C: caudal, and L: lateral. Scale bar: 200 µm.

Online Resource 8

Extent and organization of the MN group innervating the deep posterior crural muscles. (a1–a3) Photomicrographs of transverse sections from different levels of the spinal cord (as indicated in the bottom-right corner) after FG injections. (a4) 3D reconstruction of the number and distribution of MNs innervating the deep posterior crural muscles. Gray lines mark the border of the gray matter, green circles represent the central canal, and each red dot corresponds to the cell body of a single MN. White (rostralmost), blue, and yellow (caudalmost) arrows indicate the positions where the photomicrographs were taken. D: dorsal, C: caudal, and L: lateral. Scale bar: 200 µm.

Online Resource 9

Extent and organization of the MN group innervating the extensor digitorum brevis. (a1–a2) Photomicrographs of transverse sections from different levels of the spinal cord (as indicated in the bottom-right corner) after FG injections. (a3) 3D reconstruction of the number and distribution of MNs innervating the extensor digitorum brevis. Gray lines mark the border of the gray matter, green circles represent the central canal, and each red dot corresponds to the cell body of a single MN. White (rostral) and yellow (caudal) arrows indicate the positions where the photomicrographs were taken. D: dorsal, C: caudal, and M: medial. Scale bar: 200 µm.

Abbreviations

Ad9	adductor MNs of lamina 9
ALS	amyotrophic lateral sclerosis
Ant	anterior
Ax9	axial MNs of lamina 9
BAC	Bacterial Artificial Chromosome
CC	central canal
ChAT	choline acetyltransferase
CEx9	crural extensor MNs of lamina 9
CFl9	crural flexor MNs of lamina 9
Cr9	cremaster MNs of lamina 9
CV	Coefficient of variation
Dig	digitorum
DL	dorsolateral
EGFP	enhanced green fluorescent protein
ExA9	external anal sphincter MNs of lamina 9
Ext	extensor
ExU9	external urethral sphincter MNs of lamina 9
FG	Fluoro-Gold
FUS/TLS	Fused in Sarcoma/Translocated in Liposarcoma
Gl9	gluteal MNs of lamina 9
Hm9	hamstring MNs of lamina 9
HRP	horseradish peroxidase
IML	intermediolateral nucleus
Lat	Lateral
LDCom	lumbar dorsal commissural nucleus
MN	motor neuron
Pes9	foot MNs of lamina 9
Post	posterior
Q9	quadriceps MNs of lamina 9
QL9	quadratus lumborum MNs of lamina 9
SDCom	sacral dorsal commissural nucleus
SOD1	superoxide dismutase 1
Spf	superficial
TDP-43	Transactivating response element DNA binding protein-43
VL	ventrolateral

Figure 1
Click here to download high resolution image

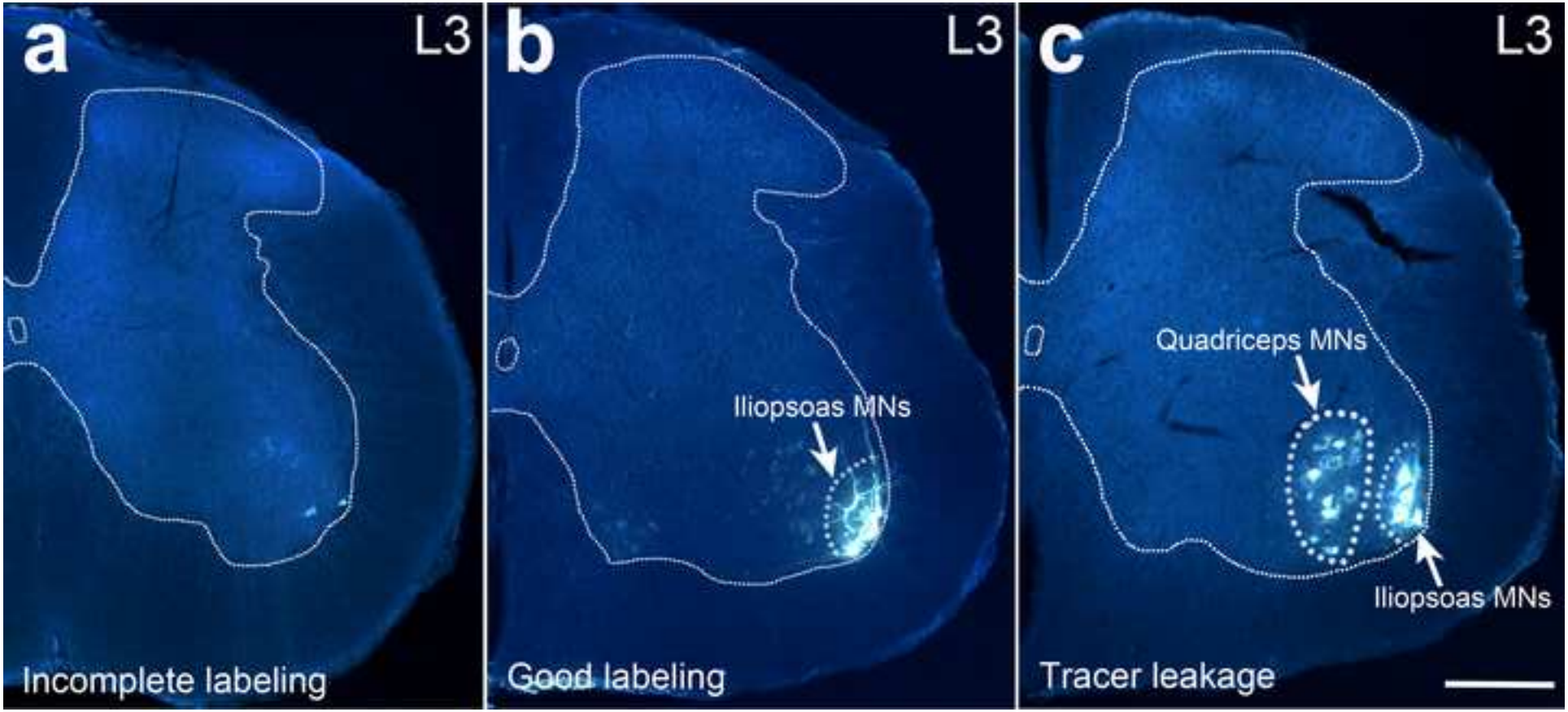

Figure 2
Click here to download high resolution image

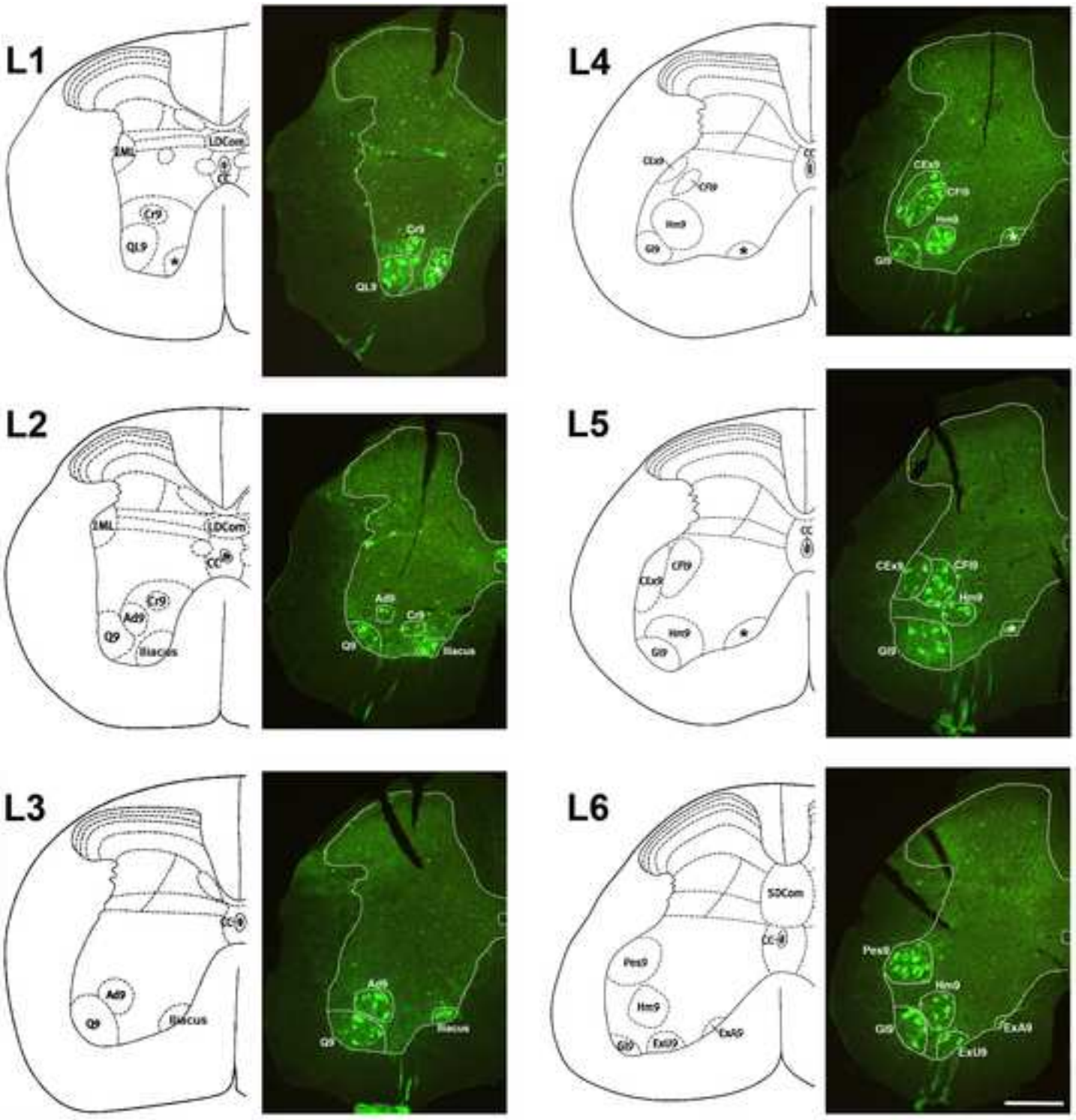

Figure 3
Click here to download high resolution image

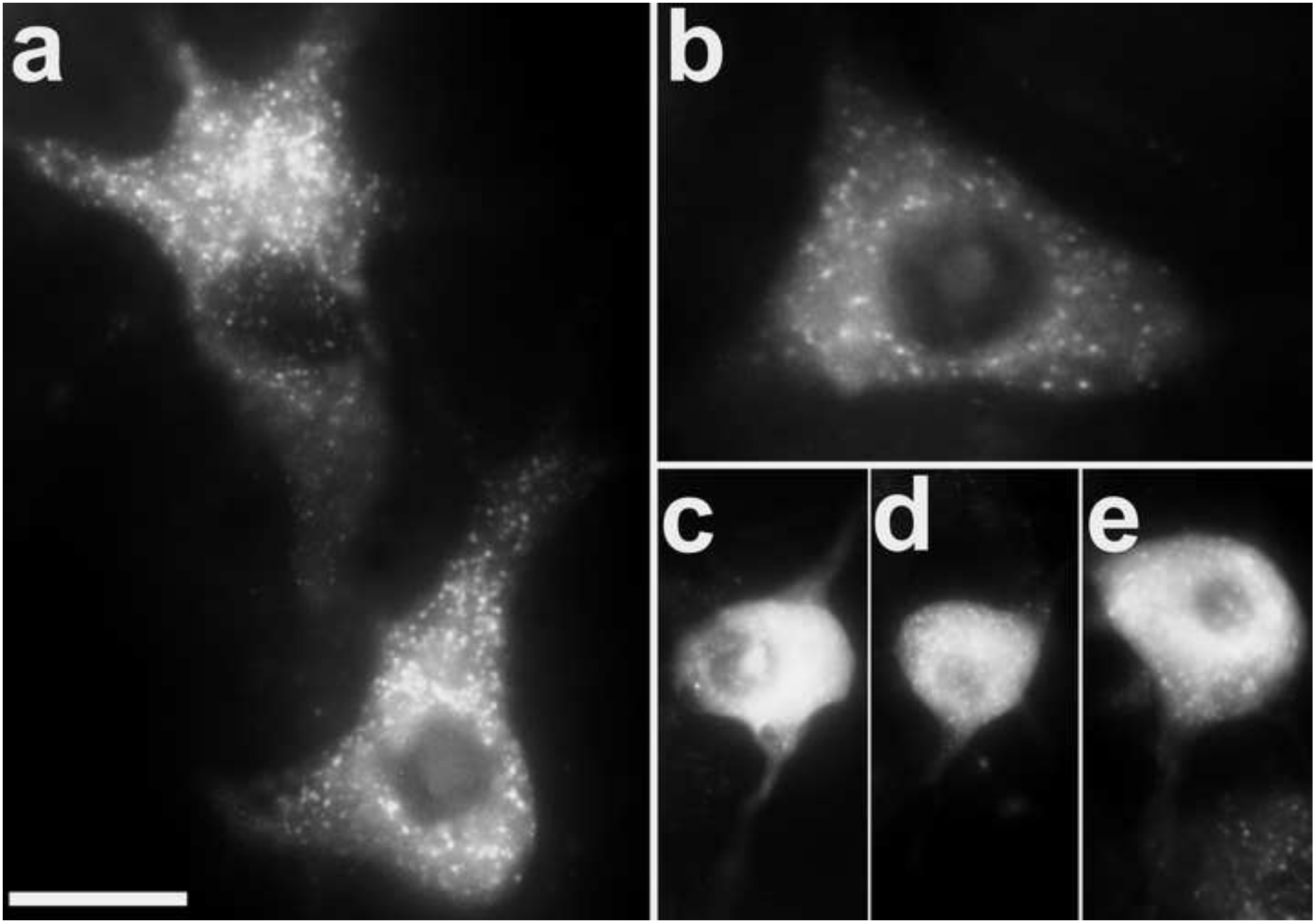

Figure 4
Click here to download high resolution image

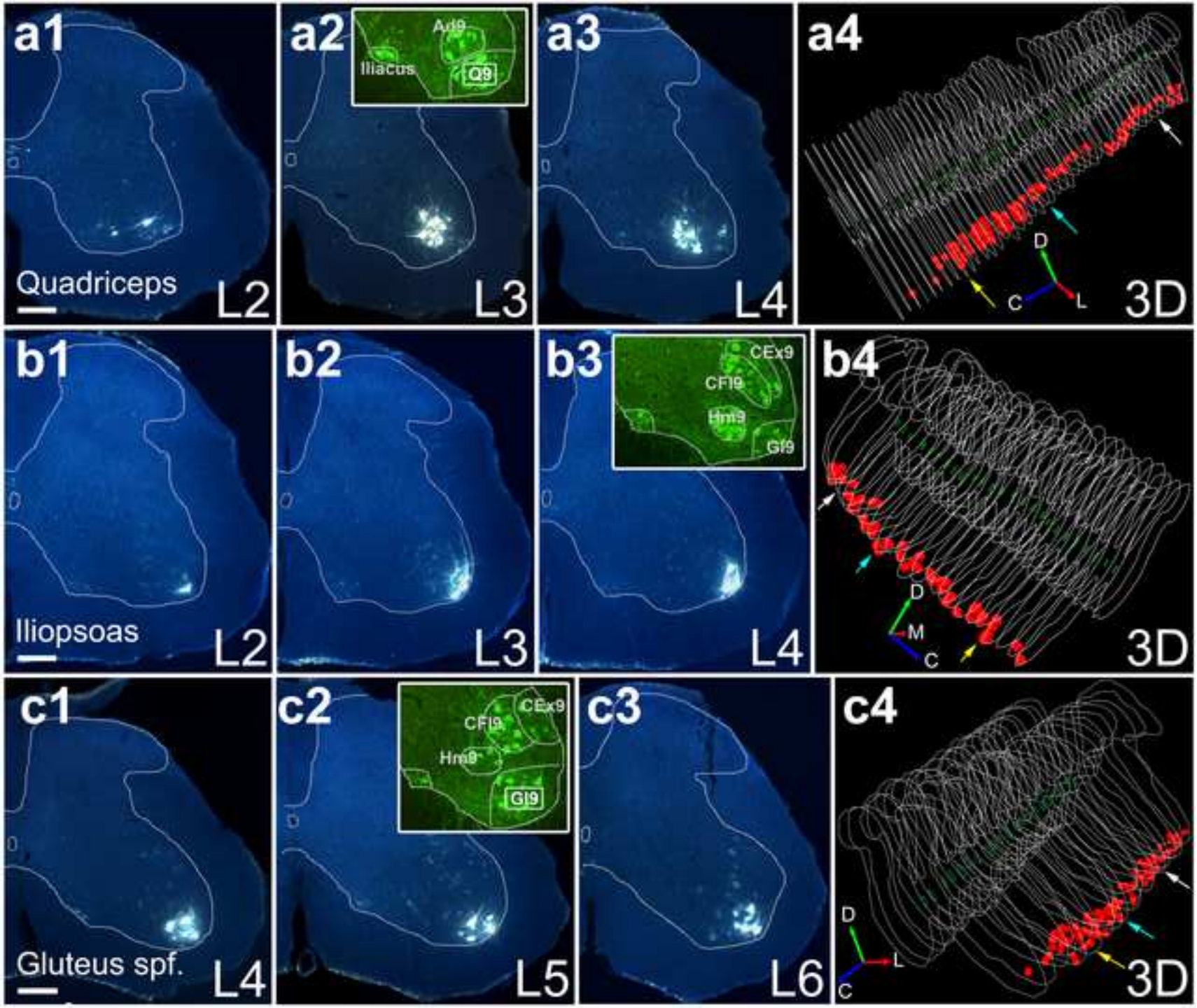

Figure 5

Click here to download high resolution image

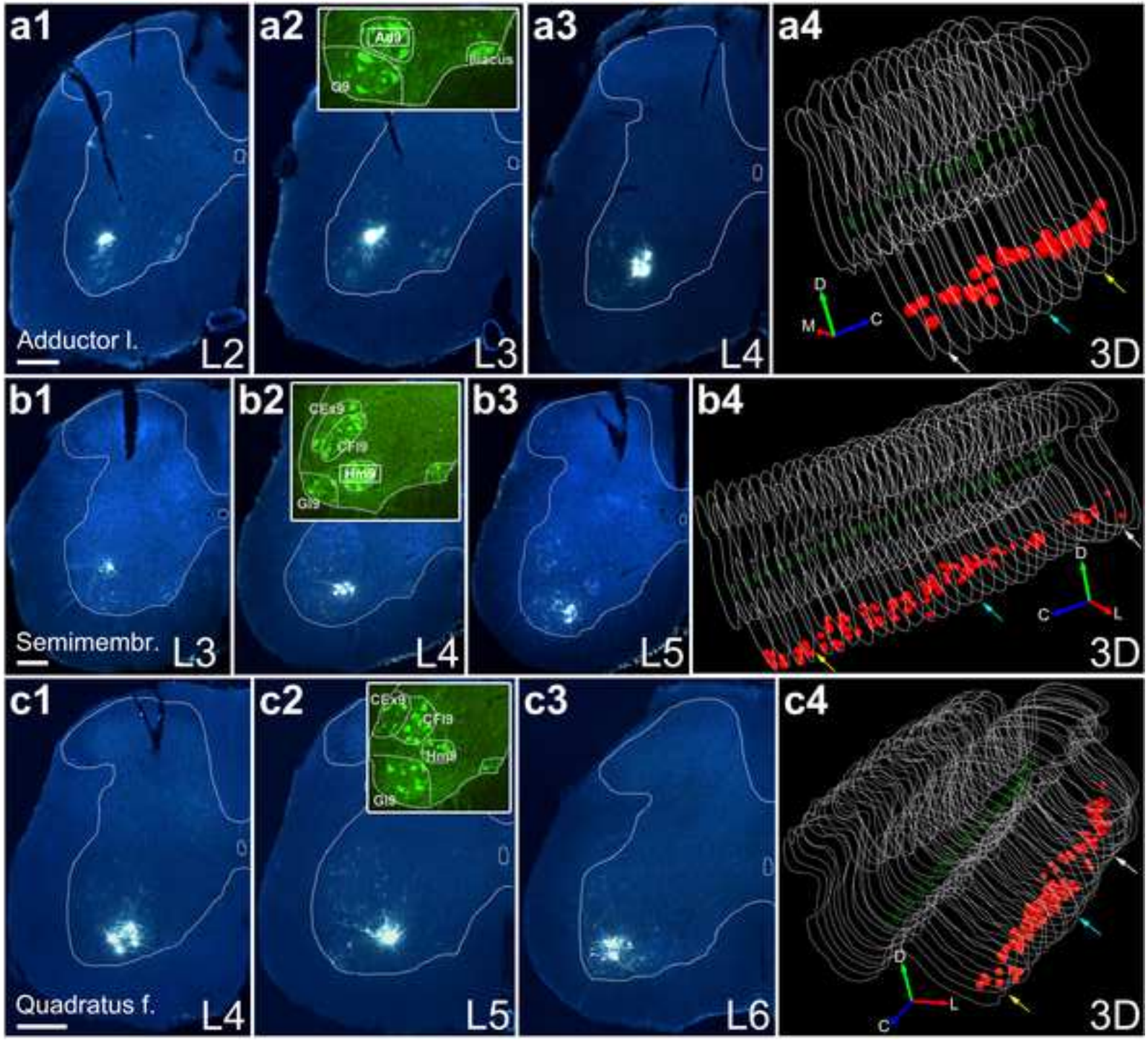

Figure 6
Click here to download high resolution image

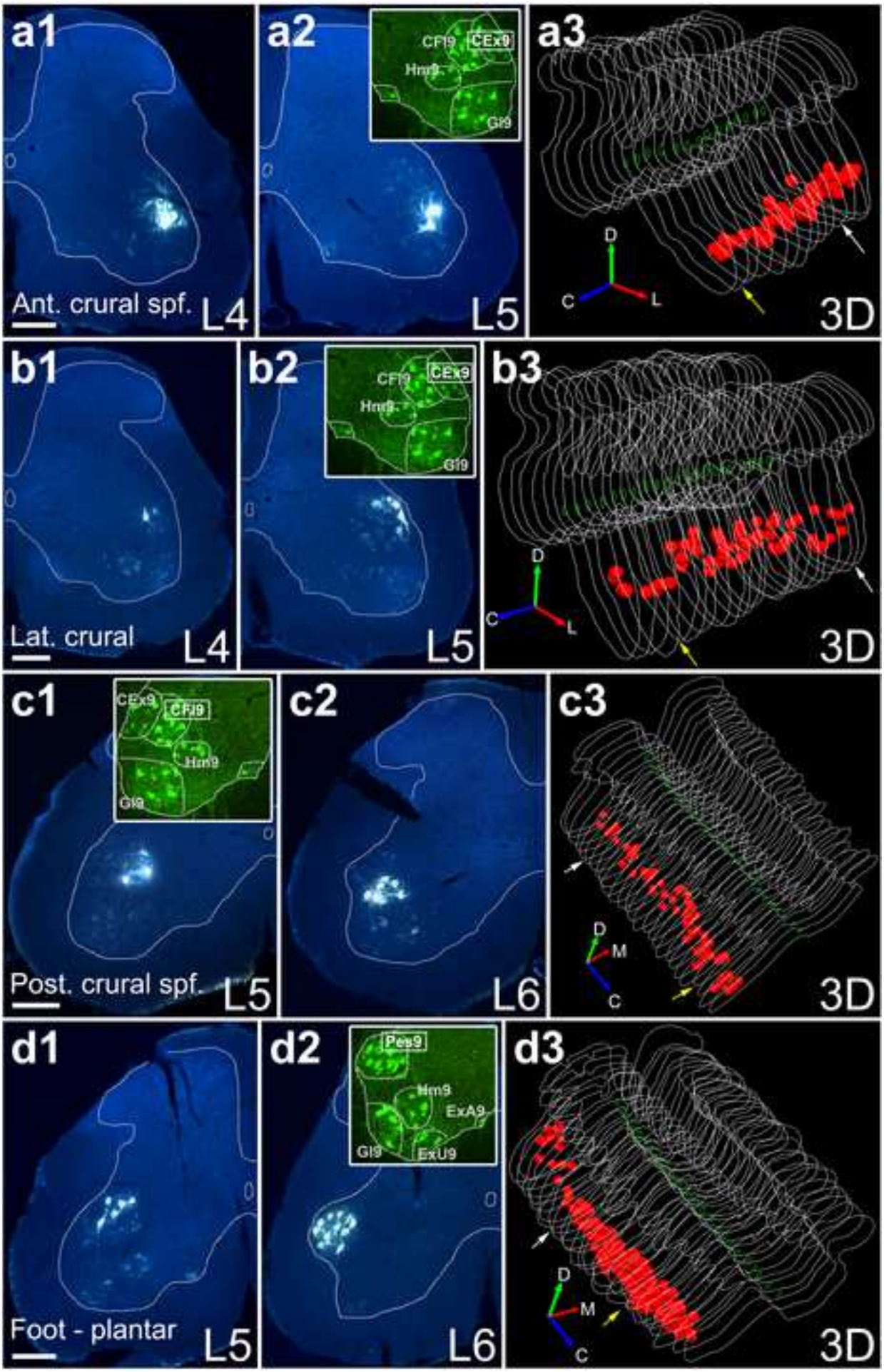

Figure 7
Click here to download high resolution image

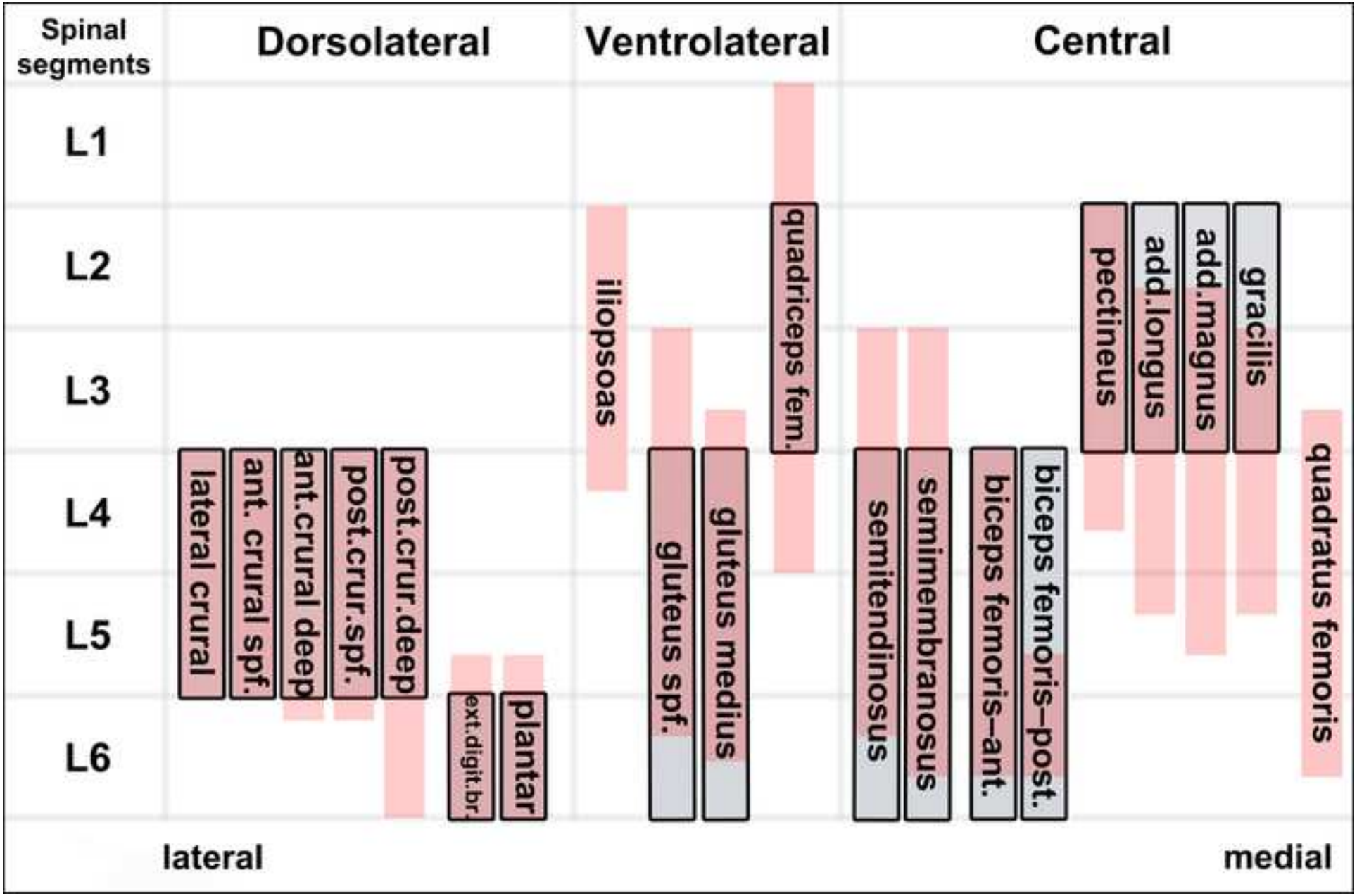

Table 1
Number and distribution of FG-labeled MNs innervating the major muscles of the mouse hindlimb

Injected muscle	Mouse ID	Total number of FG-labeled cells	Total number of FG-labeled neurons in the indicated spinal segments						Corrected number of FG-labeled cells	Average corrected number of FG-labeled cells	Motor neuron number reported by [b]McHanwell and Biscoe
			L1	L2	L3	L4	L5	L6		Mean ± S.E.M ([a]CV)	
Biceps femoris — anterior head	M3	64	–	–	–	16	41	7	52	61 ± 6 (0.16)	*[c]71 (64–79)*
	M4	87	–	–	–	–	73	14	72		
	M41	80	–	–	–	29	26	25	61		
Biceps femoris — posterior head	M16	61	–	–	–	–	46	15	48	26 ± 11 (0.74)	
	M35	17	–	–	–	–	10	7	13		
	M36	22	–	–	–	–	3	19	17		
Gluteus superficialis	M3	67	–	–	–	13	52	2	54	72 ± 9 (0.22)	*146 (109–184)*
	M4	96	–	–	3	36	57	–	77		
	M20	106	–	–	48	19	27	12	85		
Gluteus medius	M5	38	–	–	10	8	20	–	31	45 ± 11 (0.43)	
	M6	82	–	–	2	36	37	7	67		
	M21	48	–	–	–	18	15	15	37		
Semimembranosus	M7	105	–	–	28	21	32	24	83	84 ± 2 (0.05)	*58 (55–61)*
	M8	114	–	–	11	60	30	13	88		
	M9	103	–	–	1	18	33	51	80		
Semitendinosus	M7	74	–	–	22	22	26	4	57	66 ± 8 (0.22)	*[c]40 (23–52)*
	M8	111	–	–	26	57	23	5	83		
	M9	73	–	–	–	6	24	43	58		

Gracilis	M10	67	–	–	38	21	8	–	54	42 ± 6 (0.24)	*35 (27–39)*
	M11	49	–	–	27	19	3	–	39		
	M12	43	–	–	21	8	14	–	34		
Quadriceps	M11	126	13	19	88	6	–	–	102	88 ± 15 (0.33)	*172 (140–209)*
	M12	159	13	11	100	35	–	–	123		
	M21	84	9	3	53	19	–	–	67		
	M22	81	–	5	67	9	–	–	61		
Adductor magnus	M13	33	–	–	8	15	10	–	27	66 ± 21 (0.54)	*150 (130–171)*
	M14	94	–	2	9	22	61	–	74		
	M24	121	–	20	64	8	29	–	98		
Adductor longus	M16	45	–	8	25	2	10	–	36	47 ± 16 (0.58)	
	M17	36	–	3	17	13	3	–	27		
	M25	103	–	7	95	1	–	–	78		
Pectineus	M13	32	–	8	24	–	–	–	26	73 ± 19 (0.59)	*20 (13–27)*
	M14	117	3	20	91	3	–	–	95		
	M15	34	–	14	20	–	–	–	28		
	M24	150	–	17	126	7	–	–	117		
	M37	135	–	34	90	11	–	–	102		
Posterior crural superficial	M19	71	–	–	–	–	59	12	57	83 ± 25 (0.52)	*251 (208–308)*
	M25	174	–	–	–	12	58	104	133		
	M26	79	–	–	–	14	61	4	60		
Posterior crural deep	M19	144	–	–	–	12	123	9	115	144 ± 16 (0.19)	
	M29	232	–	–	–	18	105	109	170		
	M30	190	–	–	–	15	127	48	147		

Quadratus femoris	M18	53	–	–	–	38	11	4	42	58 ± 8 (0.25)	*42 (39–44)*
	M28 (left)	87	–	–	6	35	35	11	68		
	M28 (right)	83	–	–	1	33	34	15	65		
Iliopsoas	M27 (left)	28	–	4	24	–	–	–	22	28 ± 4 (0.25)	
	M27 (right)	32	–	2	20	10	–	–	26		No data
	M41	47	–	12	35	–	–	–	36		
Plantar muscles	M31 (left)	123	–	–	–	–	18	105	90	98 ± 4 (0.08)	*190 (167–219)*
	M31 (right)	137	–	–	–	–	14	123	105		
	M35	125	–	–	–	–	3	122	99		
Extensor digitorum brevis	M32	77	–	–	–	–	3	74	61	38 ± 12 (0.52)	[c]*13 (11–15)*
	M33	30	–	–	–	–	2	28	24		
	M38	40	–	–	–	–	2	38	30		
Lateral crural	M29	66	–	–	–	10	56	–	52	82 ± 15 (0.32)	
	M30	124	–	–	–	6	118	–	97		
	M38	132	–	–	–	38	86	8	97		
Anterior crural deep	M33	68	–	–	–	12	54	2	54	74 ± 22 (0.51)	
	M34	63	–	–	–	21	39	3	50		*188 (185–195)*
	M39	158	–	–	–	37	111	10	118		
Anterior crural superficial	M32	52	–	–	–	26	26	–	40	62 ± 12 (0.33)	
	M34	103	–	–	–	59	44	–	81		
	M39	86	–	–	–	42	44	–	65		

[a]CV: Coefficient of variation (calculated as standard deviation over mean).
[b]McHanwell S, Biscoe TJ (1981) The localization of motor neurons supplying the hindlimb muscles of the mouse. Philos Trans R Soc Lond B Biol Sci 293:477–508. Horseradish peroxidase tracer, 48 hrs survival. Mean (minimum–maximum).

[c]The motor neuron numbers were reported after 24 hrs survival

Table 2

Size of the cell nuclei of FG-labeled MNs innervating the major muscles of the mouse hindlimb

Injected muscle	Mouse ID	[a]Average diameter of cell nuclei (μm) Mean ± S.E.M.
Biceps femoris — ant. head	M3	9.3 ± 0.5
	M4	8.7 ± 0.4
	M41	12.1 ± 0.6
Biceps femoris — post. head	M16	10.5 ± 0.4
	M35	12.6 ± 0.5
	M36	11.4 ± 0.6
Gluteus superficialis	M3	9.2 ± 0.4
	M4	9.9 ± 0.3
	M20	9.8 ± 0.4
Gluteus medius	M5	9.1 ± 0.4
	M6	9.0 ± 0.2
	M21	11.7 ± 0.6
Semimembranosus	M7	10.4 ± 0.4
	M8	11.8 ± 0.6
	M9	11.5 ± 0.5
Semitendinosus	M7	11.7 ± 0.4
	M8	13.5 ± 0.4
	M9	10.5 ± 0.3
Gracilis	M10	10.1 ± 0.5
	M11	10.9 ± 0.3
	M12	10.1 ± 0.3
Quadriceps	M11	9.4 ± 0.4
	M12	11.9 ± 0.7
	M21	10.0 ± 0.7
	M22	13.3 ± 0.6
Adductor magnus	M13	9.0 ± 0.5
	M14	10.6 ± 0.4
	M24	9.4 ± 0.8
Pectineus	M13	9.9 ± 0.5

	M14	9.5 ± 0.2
	M15	8.7 ± 0.3
	M24	11.4 ± 0.6
	M37	12.7 ± 0.6
Adductor longus	M16	10.6 ± 0.4
	M17	12.6 ± 0.7
	M25	13.0 ± 0.9
Posterior crural superficial	M19	9.9 ± 0.3
	M25	12.5 ± 0.5
	M26	13.1 ± 0.4
Posterior crural deep	M19	10.1 ± 0.5
	M29	14.5 ± 0.5
	M30	11.8 ± 0.5
Quadratus femoris	M18	10.8 ± 0.6
	M28 (left)	11.5 ± 0.5
	M28 (right)	10.7 ± 0.4
Iliopsoas	M27 (left)	10.4 ± 0.3
	M27 (right)	9.1 ± 0.6
	M41	12.5 ± 0.4
Lateral crural	M29	10.8 ± 0.5
	M30	11.1 ± 0.3
	M38	14.3 ± 0.5
Plantar muscles	M31 (left)	14.5 ± 0.7
	M31 (right)	12.2 ± 0.8
	M35	10.5 ± 0.7
Extensor digitorum brevis	M32	10.6 ± 0.3
	M33	11.0 ± 0.5
	M38	13.0 ± 0.7
Anterior crural deep	M33	10.0 ± 0.4
	M34	10.0 ± 0.3
	M39	13.7 ± 0.6
Anterior crural superficial	M32	11.5 ± 0.7
	M34	11.0 ± 0.5
	M39	13.1 ± 0.7

[a]The mean diameter of the cell nuclei was determined on the basis of ten randomly chosen nuclei in each motor neuron pool.

Table 3
Rostrocaudal distribution of motor neuron columns innervating the major muscles of the hindlimb

Name of the muscle	Rostrocaudal position and extent of the relevant motor neuron column								
	MOUSE			[d]RAT	[e]CAT	[f]RABBIT	[g]MARMOSET[+]	[g]RHESUS MONKEY[+]	[g]HUMAN[+]
	[a]ChAT-EGFP and C57/BL6 strains	[b]Atlas of the spinal cord — C57BL strain[+]	[c]C129ReJ strain[++]						
Gluteus superficialis[A]	L3–L6	L4–L6	L3–L4	L3	L6–S1	N/A	L5	L6–L7	L5–S2
Gluteus medius[A]	L3–L6	L4–L6	L3–L4	L3	L6–S1	N/A			
Biceps femoris — anterior head[B]	L4–L6	L4–L6	L3–L4	L3–L5	L7–S1	L7–S1	L5	L6–L7	L5–S1
Biceps femoris — posterior head[B]	L5–L6	L4–L6	L3–L4	L3–L5	L7–S1	S1–S2			
Semimembranosus[B]	L3–L6	L4–L6	L2–L4	L3–L5	L6–L7	L6–L7			
Semitendinosus[B]	L3–L6	L4–L6	L2–L4	L3–L5	L6–L7	L7–S1			
Gracilis[C]	L3–L5	L2–L3	L2–L3	L1–L3	L5–L7	N/A	L3–L4	L4–L5	L3–L4
Adductor magnus[C]	L2–L5	L2–L3	L1–L3	L1–L3	L5–L7	N/A			
Adductor longus[C]	L2–L5	L2–L3	L1–L3	L1–L3	L5–L6	N/A			
Pectineus[C]	[*]L2-L4	L2–L3	L1–L2	L1–L3	L5–L6	N/A			
Quadriceps femoris[D]	L1–L4	L2–L3	L1–L3	L2–L3	L5–L6	L6–L7	L3–L4	L4–L5	L3–L4
Quadratus femoris[E]	L3–L6	N/A	L3–L5	N/A	N/A	N/A	N/A	N/A	N/A
Iliopsoas[F]	L2–L4	[#]L2–L3	N/A	L1–L2	N/A	N/A	L3–L4	L4–L5	L3–L4
Posterior crural superficial[G]	L4–L6	L4–L5	L2–L4	L3–L4	L7–S1	L7–S2	L5–L6	L6–L7	L5
Posterior crural deep[G]	L4–L6	L4–L5	L3–L5	L3–L4	L7–S1	N/A			

Lateral crural[H]	[**]L4–L5	L4–L5	L3–L4	L3–L4	L6–S1	N/A	L4–L6	L6–L7	L5
Anterior crural superficial[H]	L4–L5	L4–L5	L3–L4	L3–L4	L6–S1	L6–S1			
Anterior crural deep[H]	L4–L6	L4–L5	L3–L4	L3–L4	L6–S1	L7–S1			
Extensor digitorum brevis[H]	L5–L6	L6	L3	N/A	N/A	N/A			
Plantar[I]	L5–L6	L6	L3–L5	L4–L5	L7–S1	N/A	L6	S1	S1–S2

N/A: Data not available or not applicable

[a]Present work; [b]Watson et al. 2009a; [c]McHanwell and Biscoe 1981; [d]Nicolopoulos-Stournaras and Iles 1983; [e]Vanderhorst and Holstege 1997; [f]Portal et al. 1990; [g]Sengul et al. 2012.

[+]Assumed positions. These data are not the results of specific labeling experiments but they are based on cluster morphology.
[++]The results were obtained by intramuscular injection of HRP or by its application to the cut end of the nerve supplying the relevant muscle.
[A]Gluteal group (Gl9); [B]Hamstring group (Hm9); [C]Adductor group (Add9); [D]Quadriceps femoris (Q9); [E]Quadratus femoris (Ischiotrochanteric group); [F]Iliopsoas (Ps9); [G]Crural flexor group (CFl9); [H]Crural extensor group (CEx9); [I]Intrinsic musculature of the foot (Pes9).

[*]In one mouse (M14) three motor neurons were observed in L1. We think this may be the result of inadvertent spread of the tracer.
[**]In one mouse (M38) 6% of the labeled motor neurons (8/132) appeared in L6. We think this may be the result of spreading or individual variability.
[#]In the atlas, only the position of the psoas motor neuron group is indicated. However, the depicted position appears correspond to that of the iliacus motor neuron group on the basis of the present study.

Electronic Supplementary Material 1
Click here to download high resolution image

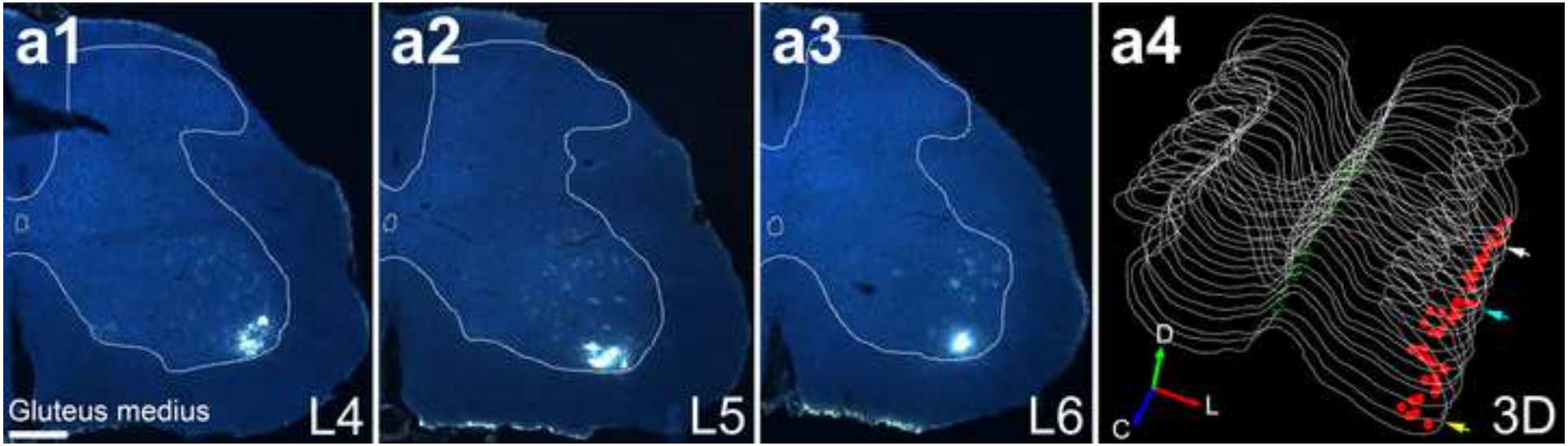

Electronic Supplementary Material 2
Click here to download high resolution image

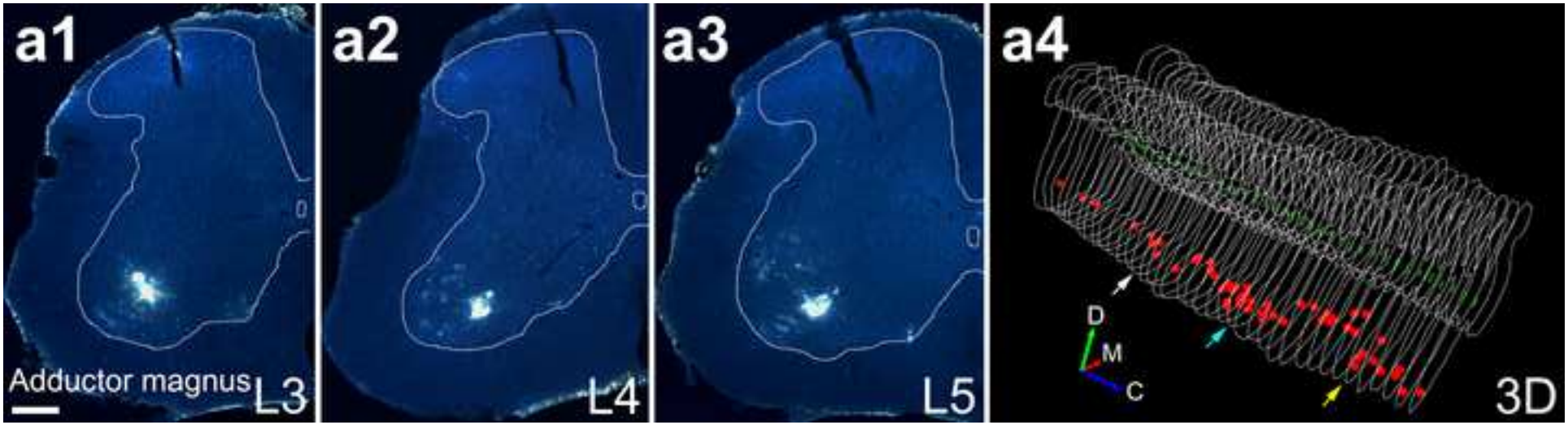

Electronic Supplementary Material 3
Click here to download high resolution image

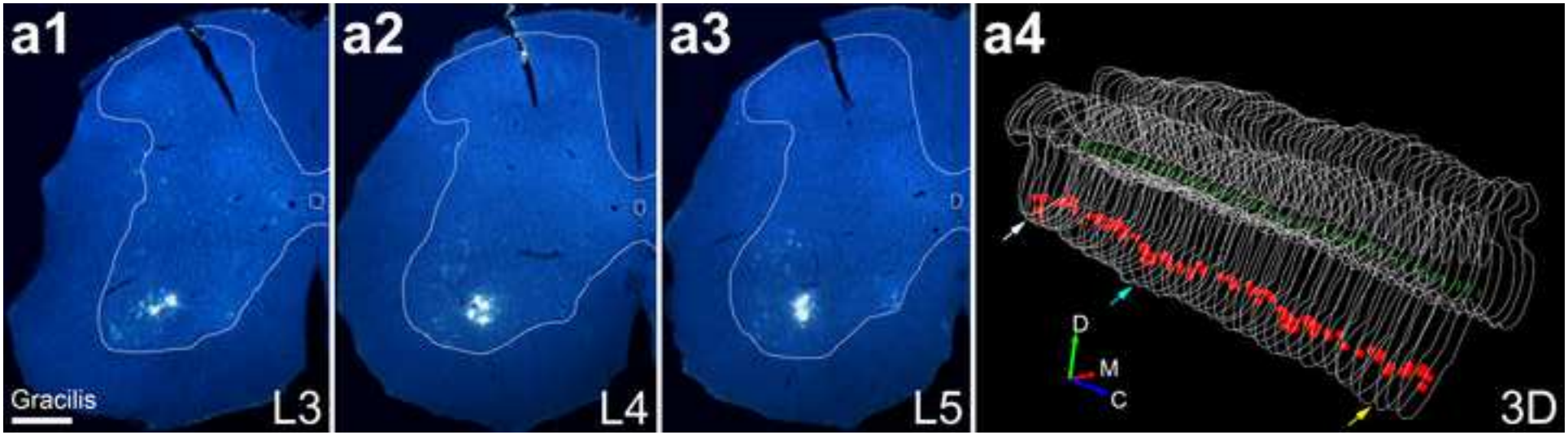

Electronic Supplementary Material 4
Click here to download high resolution image

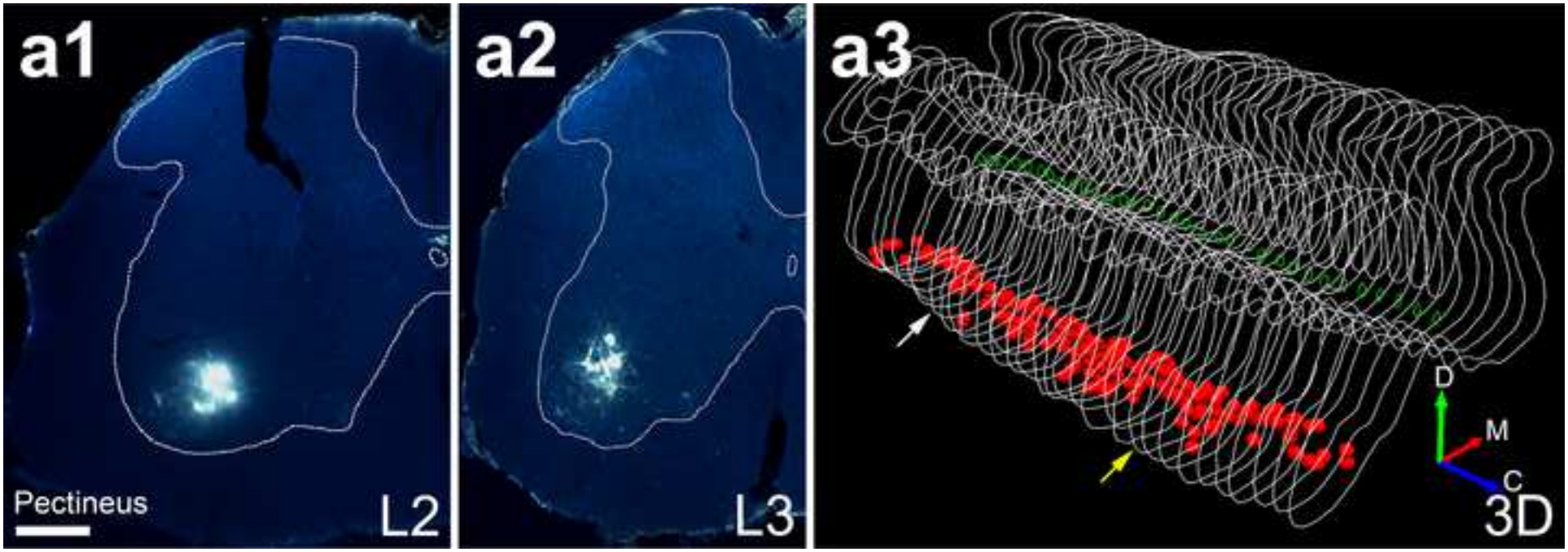

Electronic Supplementary Material 5
Click here to download high resolution image

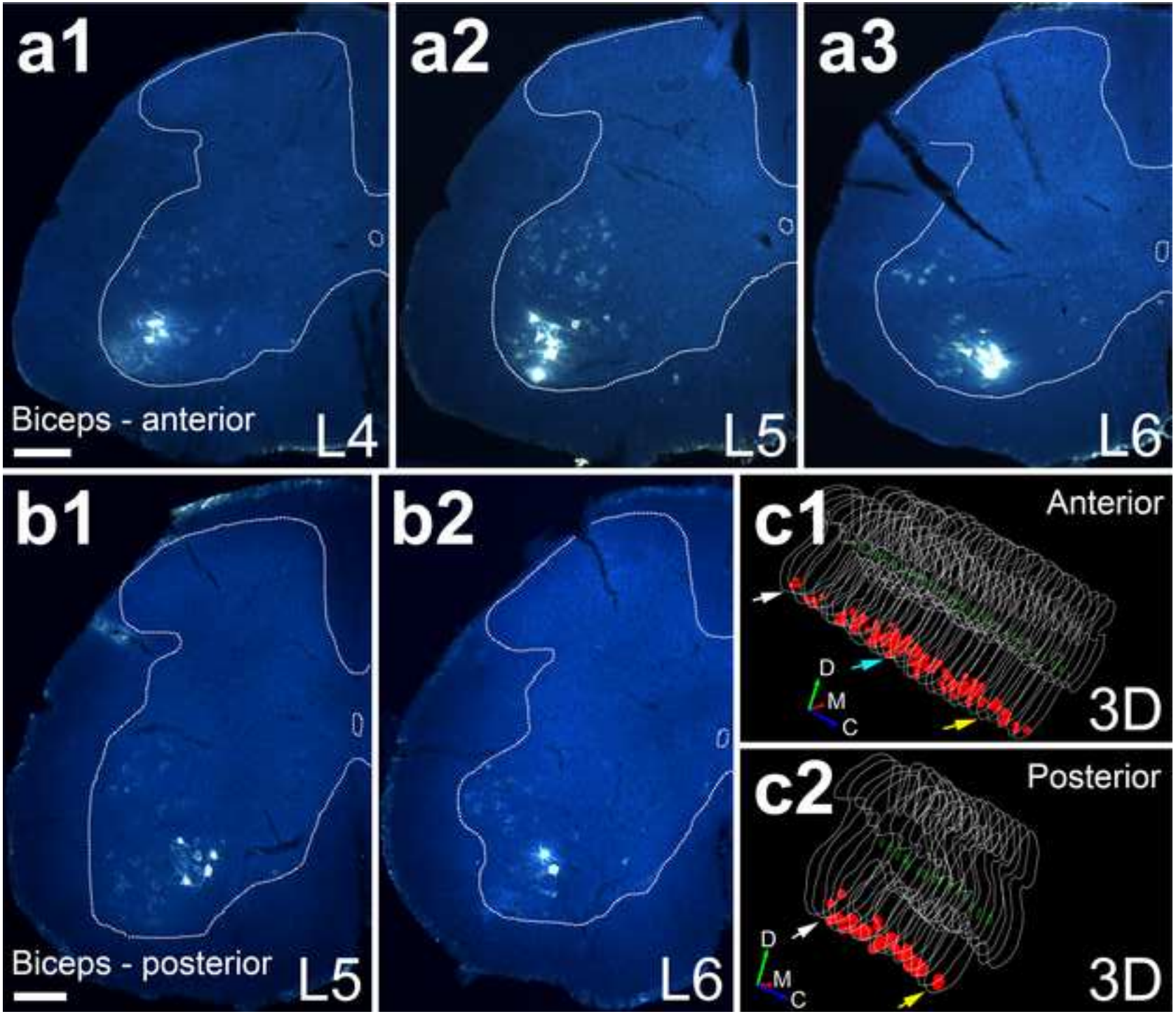

Electronic Supplementary Material 6
Click here to download high resolution image

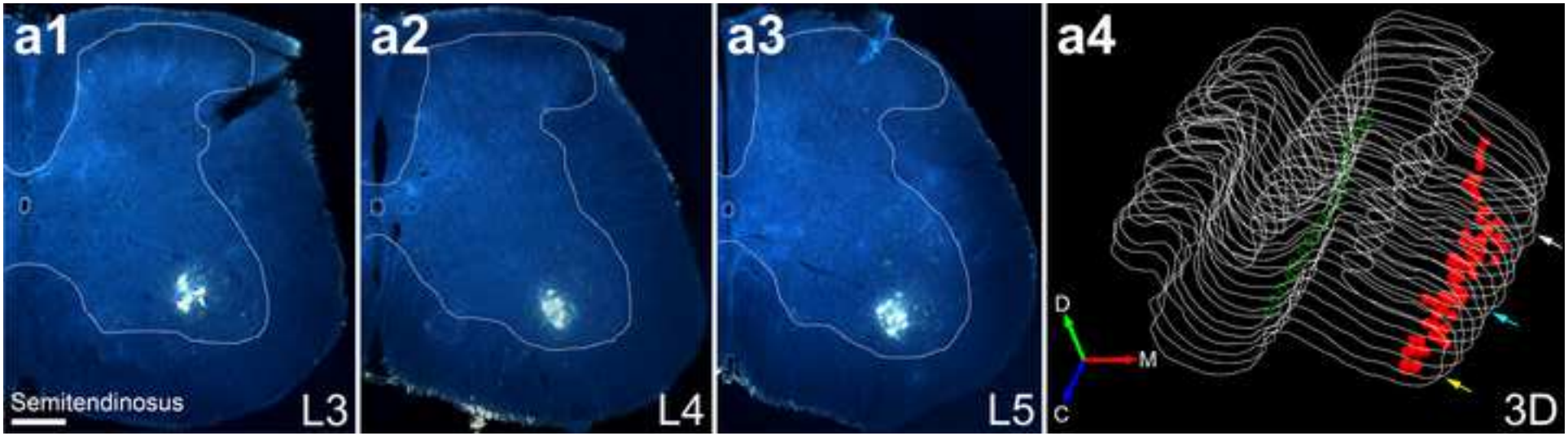

Electronic Supplementary Material 7
Click here to download high resolution image

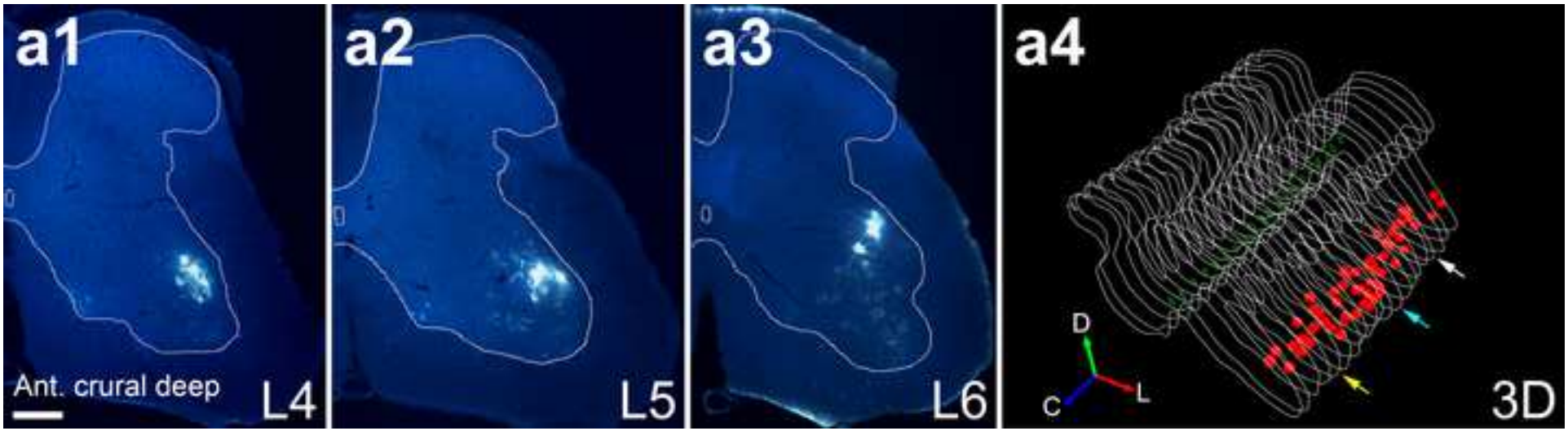

Electronic Supplementary Material 8
Click here to download high resolution image

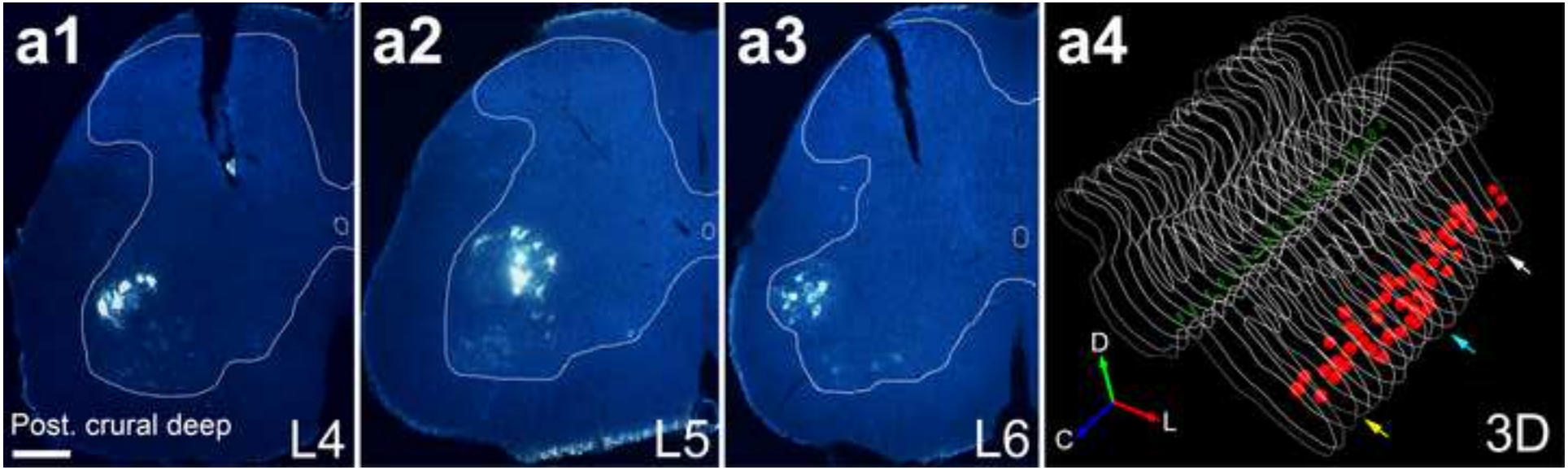

Electronic Supplementary Material 9
Click here to download high resolution image